REDOX VARIATIONS IN THE INNER SOLAR SYSTEM WITH NEW CONSTRAINTS FROM VANADIUM XANES IN SPINELS

K. Righter[1], S. Sutton[2], L. Danielson[3], K. Pando[3], and M. Newville[2].

[1]NASA-JSC, 2101 NASA Pkwy., Houston, TX 77058 (kevin.righter-1@nasa.gov)

[2]GSECARS University of Chicago, 9700 South Cass Avenue, Bldg. 434A, Argonne, IL 60439

[3]ESCG, Jacobs Engineering, Houston, TX 77058

Paper submitted as a Centennial paper for American Mineralogist, November 2015.

Revised April 5, 2016

MS 5638 R3

Abstract:

Many igneous rocks contain mineral assemblages that are not appropriate for application of common mineral equilibria or oxybarometers to estimate oxygen fugacity. Spinel-structured oxides, common minerals in many igneous rocks, typically contain sufficient V for XANES measurements, allowing use of the correlation between oxygen fugacity and V K pre-edge peak intensity. Here we report V pre-edge peak intensities for a wide range of spinels from source rocks ranging from terrestrial basalt to achondrites to oxidized chondrites. The XANES measurements are used to calculate oxygen fugacity from experimentally produced spinels of known fO_2. We obtain values, in order of increasing fO_2, from IW-3 for lodranites and acapulcoites, to diogenites, brachinites (near IW), ALH 84001, terrestrial basalt, hornblende-bearing R chondrite LAP 04840 (IW+1.6), and finally ranging up to IW+3.1 for CK chondrites (where the ΔIW notation = $\log fO_2$ of a sample relative to the $\log fO_2$ of the IW buffer at specific T). To place the significance of these new measurements into context we then review the range of oxygen fugacities recorded in major achondrite groups, chondritic and primitive materials, and planetary materials. This range extends from IW-8 to IW+2. Several chondrite groups associated with aqueous alteration exhibit values that are slightly higher than this range, suggesting that water and oxidation may be linked. The range in planetary materials is even wider than that defined by meteorite groups. Earth and Mars exhibit values higher than IW+2, due to a critical role played by pressure. Pressure allows dissolution of volatiles into magmas, which can later cause oxidation or reduction during fractionation, cooling, and degassing. Fluid mobility, either in the sub-arc mantle and crust, or in regions of metasomatism, can generate values >IW+2, again suggesting an important link between water and oxidation. At the very least, Earth exhibits a higher range of oxidation than other planets and astromaterials due to the presence of an O-rich atmosphere, liq-

uid water and hydrated interior. New analytical techniques and sample suites will revolutionize our understanding of oxygen fugacity variation in the inner solar system, and the origin of our solar system in general.

Introduction:

Oxygen fugacity (fO_2) has been recognized as an important variable in terrestrial igneous processes for decades (e.g., Osborn, 1959), and the wide range in terrestrial samples is well documented (Carmichael, 1991). On a planetary scale, oxygen fugacity can influence critical aspects of the interior and surficial reservoirs. For example, core composition is sensitive to fO_2 such that low fO_2 favors Si as an alloyed element, whereas higher fO_2 may favor O or S (Hillgren et al., 2000). The stability of metal is, of course, fO_2-dependent, and a reduced mantle may have metal as a stable phase. The FeO content or Mg# (Mg/(Mg+Fe)) of a mantle is also dependent upon fO_2 because at low fO_2 very little oxidized iron will be present and the Mg# of silicates will be high, whereas at high fO_2, FeO will be more abundant and the Mg# lower. Atmospheric composition and evolution is dependent upon fO_2 of the atmosphere as well – at low fO_2, a C-H-O atmosphere will be dominated by CH_4 and CO, whereas at high fO_2 it will be CO_2 and H_2O (Holloway and Blank, 1994). Finally, the origin of life may be dependent upon fO_2 – the pathways of complex molecule formation are sensitive to the presence of a reduced versus oxidized environment (Shock et al., 2000). Although fO_2 clearly influences magma generation processes, it is also a critical parameter for a broad range of planetary traits, and is important to understand its effects both at the micro- and macro-scale.

Igneous and metamorphic rocks commonly contain mineral assemblages that allow oxygen fugacity to be calculated or constrained, such as FeTi oxides, olivine-opx-spinel, or some other oxybarometer (Frost, 1991). Some rocks, however, contain a limited mineral assemblage and do not provide constraints on fO_2 from mineral equilibria. Good examples of the latter are orthopyroxenites or dunites: meteoritic examples are diogenites, ALH 84001, chassignites, and brachinites. In fact, it is no surprise that the fO_2 at which many of these samples formed is not

well known, other than being "reduced" and below the metal saturation value. In order to bridge this gap in our understanding, we have initiated a study of V XANES spectra in chromites from terrestrial and meteorite samples. Because the V pre-edge peak intensity and energy in chromites varies with fO_2 (Righter et al., 2006a), and this has been calibrated over a large fO_2 range, we can apply this relation to rocks for which we otherwise have no fO_2 constraints.

In this work, the results of these new measurements are interpreted in light of existing data for achondrites, as well as what we know about the fO_2 of more primitive, undifferentiated materials such as solar gas, calcium-aluminum-rich inclusions (CAIs), zoned metal grains, chondrites, cometary (Stardust) grains, cosmic dust and asteroidal (Hayabusa) particles. Effects of secondary processes such as thermal metamorphism, aqueous alteration, and low-pressure differentiation are assessed, and comparisons are made to redox variations on larger bodies such as Earth, Mars, Mercury and Moon. These latter bodies have experienced degassing, volatile solubility, fractionation, assimilation, and ascent across a wider range of pressures, and direct comparison to fO_2 measured in achondrite bodies will allow the effect of pressure on fO_2 to be evaluated.

Samples

We have selected a suite of samples for which there are no appropriate phases for application of standard oxybarometers, and for which there are large and accessible chromites. ALH84001 is a martian orthopyroxenite (Fig. 1a), for which there has been some debate regarding its oxygen fugacity; some have argued for a relatively high fO_2 near the fayalite-magnetite-quartz (FMQ) buffer (Herd et al., 2001), while others have argued for a more reduced value, well below FMQ (Righter and Drake, 1996; Righter et al., 2008a). Brachinites are olivine-rich achondrites that also contain chromite, plagioclase and pyroxene. They have recently been linked

to the ungrouped achondrite GRA 06128/129 through similarity of O isotopes, age, and composition (Shearer et al., 2008; Ash et al., 2008; Zeigler et al., 2008). Chromites in the brachinites EET 99402 and ALH 84025 (Fig. 1b) were measured and compared to those in GRA 06128 to assess whether they record comparably oxidized conditions. Diogenites contain orthopyroxene and chromite, and have been linked to eucrites and the HED parent body, which is thought to be at ~ IW-1 (Stolper, 1977; Hewins and Ulmer, 1984). We have measured chromites in the diogenites ALH 77256 and GRA98108, and can compare the results to previous estimates related to the HED parent body. CMS 04071 is a main group pallasite with coarse-grained chromite that we analyzed for this study (Danielson et al., 2009). We have also analyzed chromite from a lodranite (EET 84302) and acapulcoite (MET 01198) again because the redox conditions in this parent body have not been discussed in detail, yet are of fundamental importance in understanding and constraining the processes that led to their formation. Among chondrites, we have analyzed chromian magnetites from CK chondrite QUE 99679, and chromite from the amphibole-bearing R chondrite LAP 04840 (Fig. 1c).

In addition to the meteorite samples above, we analyzed spinel inclusions in olivine from three basalts from the Mexican volcanic belt (MVB) – Michoacan-Guanajuato volcanic field (MGV-19; Figure 1d), Sierra Chichinautzin (TMV-6), and San Martin Tuxtla (SMT-1) (Righter et al., 2008b).

XANES and EMPA measurements

All major elements in spinels were analyzed with a CAMECA SX100 electron microprobe, using an accelerating voltage of 20 kV, sample current of 20 nA, and standardization and corrections as described in Righter et al. (2006a). Measurements of the valence of V were made using

synchrotron micro-XANES (***X***-ray ***A***bsorption ***N***ear-***E***dge ***S***tructure) spectroscopy (SmX), at the Advanced Photon Source (APS), Argonne National Laboratory (beamline 13-ID, the Consortium for Advanced Radiation Sources or CARS). SmX measurements are made by focusing a monochromatic (cryogenic, Si (111) double crystal monochromator) X-ray beam (3x3 μm) from the synchrotron onto a spot on the sample and measuring the fluorescent X-ray yield from that spot as a function of incident X-ray energy. Changes of fluorescent X-ray intensity and energy of features in the XANES spectrum (notably the pre-edge peak) depend on oxidation state and coordination (e.g., Wong et al., 1984; Sutton et al., 2005; Righter et al., 2006a).

Previous work on XANES-based oxybarometers has utilized correlations between the V K pre-edge intensity and either V valence (e.g., glasses of Sutton et al., 2005) or oxygen fugacity (spinels of Righter et al., 2006a). In this study, the correlation between oxygen fugacity and V pre-edge peak in spinel documented by Righter et al. (2006a) (Figure 2), is used to calculate fO_2 from the pre-edge peak intensity from each spectrum (Table 1). Most discussions of oxygen fugacity in this paper utilize the ΔIW notation which is the $\log fO_2$ of a sample (at T) relative to the $\log fO_2$ of the IW buffer (at T). Because many buffered equilibria are parallel to each other in temperature-$\log fO_2$ space due to the temperature dependence of enthalpy, the ΔIW is largely independent of temperature and is thus a convenient way to compare fO_2 conditions of many materials, both solid and liquid (e.g., Carmichael and Ghiorso, 1990). One fit to the ΔIW and pre-edge peak intensity data uses a five-parameter exponential function to fit the data between IW-1 and IW+9, with a standard error in the estimate of 0.78. A second fit uses only data with pre-edge peak intensity between 0 and 100 to more closely match the data from the natural samples measured here, and results in a standard error of 0.62. Results from both of these fits are tabulated in Table 1, in log units relative to the IW buffer. We use the values from the second fit in

all of the discussion because of the more focused range, and because of the higher error associated with the first fit which is due to some scatter in data from high fO_2 that are not relevant to the samples in this study.

XANES spectra of single anisotropic crystals can be sensitive to orientation relative to the x-ray beam (e.g., Dyar et al., 2002); however, such effects in spinels are expected to be negligible because they are isotropic (Righter et al., 2006a). Extensive work on glasses has shown that the pre-edge intensities are also dependent upon temperature. We have no evidence for temperature dependence in spinels, but a systematic examination is lacking and could be the focus of future efforts. Additionally, dependence of V and Cr XANES spectra on compositional variation in glasses (Sutton et al., 2005) and olivines (Bell et al., 2014) is known to be important. Crystal chemical controls on spinel chemistry are well known (e.g., Papike et al., 2004, 2015), but no such compositional or structural dependence for XANES spectra is known yet for spinels - this could also be a fruitful avenue for future research.

Results

The V pre-edge peak intensity for all samples measured ranges from 14 at the low end (defined by the acapulcoite-lodranite group) to ~ 75 at the high end (defined by the CK chondrite QUE 99679). There is a general progression from reduced to oxidized from the acapulcoites to diogenites to GRA 06128 to brachinites to ALH 84001 to terrestrial basalts to the CK chondrites (Fig. 3). There are several noteworthy points here, including both comparisons to previous results, and new fO_2 observations on samples of previously uncharacterized or debated origin.

The values just below the IW buffer for the CMS pallasite are in good agreement with the calculated and measured fO_2 for pallasites reported by Righter et al. (1990), and diogenite ΔIW

values calculated here are similar to estimates made previously for eucrites (Stolper, 1977), and for the HED parent body (Righter and Drake, 1996). The lodranite-acapulcoite suite seems very reduced, perhaps as much as 2 log fO_2 units below the IW buffer, in agreement with previous estimates (Righter and Drake, 1996; McCoy et al., 1997). The results for the R chondrite LAP 04840 yield values between IW-0.5 and IW+1.6, in agreement with previous work on R chondrites, which ranges between IW-0.5 to IW+2.56 (Righter and Neff, 2007). CK chondrite spinels are the most oxidized, also in agreement with the calculations of Righter and Neff (2007). Finally, the spinel inclusions in terrestrial olivine basalt phenocrysts exhibit a range of values from IW+3.42 (TMV-6b) to IW+1.1 (SMT-1) to IW+0.4 (MGV-19). The value for TMV-6b is close to that expected from olivine-melt equilibria (IW+2.6; Righter et al., 2008b) suggesting that little to no oxidation occurred between the time of trapping of spinel to later magma emplacement. On the other hand, the values measured in SMT-1 and MGV-19 are much lower than those derived from bulk rock FeO/Fe_2O_3 (IW+4.7 and IW+4.2, respectively), indicating that these samples became oxidized subsequent to chromite crystallization, perhaps during emplacement or eruption.

Results for GRA 06128 (IW-0.7 to IW-1.05) and the brachinites (ALH 84025 and EET 99402; IW-0.5 to IW+0.4) are relatively oxidized, but distinctly different from each other, with the GRA 06128 samples slightly lower than the brachinites. These samples are all more oxidized than the acapulcoites, lodranites, and GRA 98108 diogenite, however, which suggests that they may have come from a more oxidized parent body. ALH 84001 is more oxidized (IW+0.5) than these metal-bearing meteorites, but more reduced than most of the terrestrial basalts that have equilibrated at IW+0.26 to IW+3.42. Our results are consistent with values of FMQ-2.7 (IW+0.9) estimated for ALH 84001 by other techniques such as mineral equilibria or Eu/Gd par-

titioning in pyroxenes (Herd et al., 2001), but inconsistent with values as high as FMQ (IW+3.5) reported by Wadhwa (2008).

Overall, there is a correlation of Mg# with oxidation state of V that is consistent with the general idea of oxidation in the presence and absence of metal (Fig. 4). At low fO_2, there is less FeO (and more Fe) available so olivines and pyroxenes are more magnesian. At intermediate fO_2 there is ample FeO so that silicates have lower Mg#, but at still higher fO_2, FeO becomes less abundant and Fe_2O_3 more abundant, again forming magnesian silicates. This sequence, from Fe to FeO to Fe_2O_3 with oxidation, causes the C-shaped trend seen in Figure 4.

Techniques for estimating oxygen fugacity

Oxygen fugacity has traditionally been defined or calculated using thermodynamic data for various equilibria such as simple metal-oxide equilibria, or more complicated equilibria involving multiple phases or minerals (Chase, 1986; Robie et al., 1978). Such equilibria can be studied using experimental techniques as well, such as electrochemical measurements. The emf of simple and complex equilibria have been measured for a wide variety of terrestrial and planetary materials, but results can be compromised by contamination with C or other elements that can influence the equilibria being studied. Nonetheless, careful studies have placed important constraints on oxygen fugacity in some planetary sample suites such as the Skaergaard intrusion (Kersting et al., 1989), CAIs (Kozul et al., 1988), and pallasites (Righter et al., 1990). Experimental studies have been used to constrain or bracket fO_2 in certain samples such as eucrites (Stolper, 1977), angrites (Jurewicz et al., 1993), CAIs (Grossman et al., 2008), or martian meteorites (Xirouchakis et al., 2002), by investigating phase equilibria at different fO_2. Experimental studies can also help to constrain the influence of fO_2 on trace element partitioning and thus indi-

rectly determine fO_2 on the basis of partitioning of these elements in natural systems (Papike et al., 2013). For example, Eu partitioning between pyroxene and melt has been used to constrain fO_2 in eucrites, shergottites, and lunar basalts (Shearer et al., 2006a), and Ce has been used to constrain fO_2 in zircon-bearing Archean rocks (Trail et al., 2011).

Modern analytical approaches have provided additional ways to constrain fO_2. X-ray absorption near edge structure (XANES) spectroscopy, which is available at synchrotron facilities (Bassett and Brown, 1990) has allowed the study of valences of elements, such as Fe, V, Cr, Mn, Mo, W, Ti, S, and P, that have multiple valence states in many planetary materials. In particular, the valences of Fe, Ti, V, and Cr have been applied to planetary materials and provided information on a microscopic scale. Transmission electron microscopy can be used with electron energy loss spectroscopy (EELS) to determine the valences of Fe and Mn (e.g., Garvie and Buseck, 1998; Zhang et al., 2010), and this approach has been used to determine fO_2 in, for example, martian meteorites and Stardust comet particles (Herd et al., 2001; Stodolna et al., 2013).

These are a few of the approaches that have been used to constrain fO_2 in planetary samples, and all of them are represented in the comparative discussions below involving nebular and primitive materials, chondrites, achondrites and planets. These comparisons will utilize ΔIW, which is defined above.

Oxygen fugacity recorded in natural materials

Primitive materials

We can compare the fO_2 of the solar nebula to those found for a wide range of materials that occur in primitive meteorites, cosmic dust and comets (Figure 5). In this context "primitive" refers to materials that have not been thermally or aqueously altered. Chondrites contain four ma-

jor components: inclusions such as CAIs and AOAs (amoeboid olivine aggregates); chondrules; matrix; and metal – and they each can place constraints on the fO_2 of their formation.

Solar fO_2 values

The fO_2 of the solar nebula can be defined using both theory and samples. The solar C/O ratio can be used to constrain the fO_2 of the solar nebula, and using a value of C/O = 0.5 (Allen-de-Prieto et al., 2002) leads to a nebular fO_2 of IW-6.8 (Fig. 5; Grossman et al., 2008). The fO_2 of the solar nebula has also been constrained by experimental studies. The fO_2 of a gas in equilibrium with the liquid from which CAI composition melilite and Ti^{3+}-bearing fassaitic pyroxene crystallize is about 1 log fO_2 unit below the fO_2 defined by a solar C/O = 0.50 ratio (Grossman et al., 2008). These very low fO_2 values will form the basis of a comparison of other primitive materials found in chondrites, comet and primitive dust particles (Fig. 5).

Refractory Inclusions (CAI/AOA)

Calcium-aluminum-rich inclusions (CAIs) have been used to estimate oxygen fugacity in the solar nebula, yielding a wide range of values, depending on the meteorite type. Paque et al. (2013) found Ti valence between 3.5 and 4.0 in spinel in CV3 chondrites. Paque et al. (2013) concluded that although some CAIs show evidence for conditions as reduced as IW-8, there is also evidence for transient oxidation to values as high as IW-2.5, so that the more reduced, primitive values may have been changed during nebular processing (Fig. 5). Processing may be common, based on Simon et al. (2005), and additional work of Dyl et al. (2011) and J. Simon et al. (2011), in which there is evidence for variation within the rims of CAIs (Fig. 5). Finally, Ihinger and Stolper (1986) showed that blue hibonite in Murchison contains Ti^{3+} and that the hibonite is blue when it is synthesized at 1430 °C between log fO_2 = -10.7 and -15.0 (ΔIW = -

5.6 to -1.3). This range of fO_2 extends to nearly solar values, showing that the blue hibonite could have formed in equilibrium with a gas of nearly solar composition (Fig. 5).

Chondrules

Examining simple equilibria between metal and olivine in chondrules from a wide range of primitive chondrites (E, C, O), Zanda et al (1994) demonstrated that the fO_2 under which these chondrules formed ranged from IW-4 to IW-0.5 (Fig. 5). Connolly et al. (1994) proposed that this range was caused by carbon acting as a reductant across a range of pressures, given the sensitivity of graphite saturation to pressure. Using a similar approach, Schrader et al. (2013) examined Type I and Type II chondrules in CR chondrites and also found a range of values, from IW-4 to IW-0.5 (Fig. 5). Measurements of the chromium oxidation state in olivine from a chondrule in an EL3 chondrite showed that it is entirely Cr^{2+}, which implies a very low fO_2, certainly lower than IW-1 (Hanson and Jones, 1998) and possibly even near solar values of IW-6 (McKeown et al., 2014). Examination of Ti^{3+} in olivine in chondrules from ordinary chondrites reveals less Ti^{3+}, but it is still present (S. Simon et al., 2015) and may indicate that their precursors formed in reducing environments, and that they contain reduced Ti that survived chondrule formation in an environment where Fe^{2+} was stable (Simon et al., 2013).

Finally, the mineralogy of enstatite chondrites - Si-bearing metal, oldhamite, niningerite, pure silica and albitic plagioclase in addition to enstatite and minor olivine – is traditionally accounted for by condensation from a gas of solar composition but at a higher C/O ratio (0.83) and therefore more reduced than solar gas, at IW-8 to IW-10.5 (Grossman et al., 2008; Grossman et al., 1979; Lehner et al., 2013). However, studies of Ti valence in olivine and pyroxene from enstatite chondrites show a larger stability field for Ti^{4+} than expected, and Lusby et al. (1987) observed FeO-rich phases in enstatite chondrites. Both of these suggest that enstatite chondrites

may have formed initially from an oxidized reservoir and then become reduced later (Simon et al., 2013). It is possible that enstatite chondrites have experienced variable fO_2 conditions in their formation, or contain components with complex histories.

Metal

CH, CR and CB chondrites contain FeNi metal grains that are zoned from core to rim in many trace siderophile elements. Those patterns are best explained by condensation from a nebular gas at an fO_2 of IW-6, about 1 log fO_2 unit above solar values (Petaev et al., 2003) (Fig. 5); metal grains in some CB chondrites may result from condensation from an impact generated plume rather than solar nebula (Campbell et al., 2002; Fedkin et al., 2015). In addition, there are some refractory metal grains in CV3 chondrites that have trace siderophile element abundances consistent with condensation from a gas of solar composition but at an fO_2 (defined by H_2O/H_2 ratio) of IW-4 (Palme et al., 1994). Additional grains from the same study also showed evidence for formation at more oxidized conditions, again (as with some CAI above; Paque et al., 2013) suggesting more transient and oxidizing conditions in the early solar nebula (Fig. 5).

Matrix

Many carbonaceous chondrites contain a significant amount of matrix material and recent studies have shown that the matrix is much more oxidized than some of the other components such as chondrules, metal and inclusions. For example, Le Guillou et al. (2015) found that the matrices of many primitive CR chondrites have $Fe^{3+}/\Sigma Fe$ values from 0.6 to 0.7. Also, the matrices of many aqueously altered CM and some CV meteorites contains fayalite-rich olivine that is hypothesized to have formed under relatively oxidizing conditions (Zolotov et al., 2006).

Comets and cosmic dust

Comet particles returned by the Stardust mission have revealed some interesting features related to oxidation. Much of the material characterized from the Stardust mission is relatively oxidized and fine-grained (e.g., Stodolna et al., 2013; Westphal et al., 2009; Ogliore et al. 2010; Simon et al., 2008), but equating oxidation states with a specific fO_2 has not been done quantitatively because much of the material is polycrystalline, there has not been a detailed calibration of the fO_2 and $Fe^{3+}/\Sigma Fe$, and also because some of the materials were modified during the collection process (e.g., Leroux et al., 2008; 2009). Several Stardust particles have been characterized in great detail and appear to have formed either close to or just above the IW buffer. Nakamura et al. (2008) studied the Torajiro particle and found that it equilibrated at IW+1.4. Gainsforth et al. (2015) studied the olivine-chromite aggregate particles Iris and Cali and found evidence suggesting an fO_2 of formation at IW-0.3 based on thermodynamic calculations of olivine, glass, and chromite equilibria in Iris, and found chromite in Cali with $Fe^{3+}/\Sigma Fe$ = 0.13. Similar mineralogies have been reported in the KOOL (KO = kosmochloric Ca-rich pyroxene, OL = olivine) particle Puki-B as well (Joswiak et al., 2009). On the other hand, a CAI-like particle characterized by Simon et al. (2008) called Inti was estimated to have formed near IW-6 (Fig. 5), more reduced than many other particles.

Cosmic dust particles examined by Ogliore et al. (2010) also appear to be more oxidized like some Stardust particles and chondritic matrix. On the other hand, GEMS (glass with embedded metal and sulfides) grains found within cosmic dust particles exhibit overall reduced phases, with the glass containing iron predominantly as FeO with no Fe_2O_3 (Keller and Messenger, 2011), and ranging from 2.5 to 15 wt% FeO (Bradley, 1994). Metal-oxide equilibria for GEMS could thus have equilibrated have equilibrated below the IW buffer, from ΔIW = -1.2 to -2.8 given the range of FeO measured (Fig. 5). Altogether, the Stardust materials and cosmic dust

particles exhibit a range of fO_2 conditions from near solar (Inti) to very oxidized (GEMS, Torajiro, and Cali).

Thermal and aqueous alteration in chondrites

Many chondrite groups exhibit evidence for heating or thermal metamorphism to temperatures as high as 1000 °C. Such metamorphism is recorded in the ordinary chondrites (H, L, and LL 4 to 6; van Schmus and Wood, 1967), in enstatite chondrites (EL4 to EL6; EH4 to EH6; Zhang et al., 1995) the CK carbonaceous chondrites (CK4 to CK6; Kallemeyn et al., 1991), and in the R chondrites (R4 to R6; Bischoff et al., 2011). A systematic study of fO_2 in thermally metamorphosed H ordinary chondrites was done by Kessel et al. (2004), who found that H4 to H6 chondrites equilibrated at IW-2.2 to 2.5, and that H6 were <0.2 log fO_2 units more oxidized than H4 - a very small effect if any. LL and L chondrites contain silicates richer in FeO than those in H chondrites, and they equilibrated at slightly higher fO_2s than H chondrites, probably near IW-1.5 to IW-2 (Righter and Drake, 1996). Particles were collected from asteroid Itokawa, which is of LL parentage, by the Hayabusa spacecraft. The particles exhibit a range of petrologic type from 4 to 6, and their olivine, low-Ca and high-Ca pyroxene Fe XANES spectra are identical to those of the LL5 chondrite Tuxtuac (Noguchi et al., 2013). Similarly, the thermally metamorphosed EH and EL chondrites share the reduced mineralogic characteristics of their unequilibrated relatives. CK chondrites also show a range of textural evidence for petrologic type 4 to 6, but detailed mineralogic studies show a rather limited mineralogic variation, suggesting that either the CK thermal history had a relatively restricted range of temperatures, or that the higher-grade samples experienced retrograde metamorphism (Righter and Neff, 2007). Overall, the CK chondrites are much more oxidized than other chondrite groups – they lack metal, con-

tain magnetite, and have olivine with lower FeO contents than those in LL or other metal-bearing oxidized chondrites; given the presence of magnetite, this is consistent with the oxidation of FeO to Fe_2O_3. The magnetites exhibit V K pre-edge peak intensities from near 70 to 75, indicating equilibration near the FMQ buffer (IW+3.5). In general, thermally metamorphosed chondrites do not exhibit evidence for oxidation accompanying the metamorphism (e.g., Simon et al., 2015). CK chondrites are oxidized, but may have started oxidized; hopefully more CK3 samples will be recovered in the future, and this will become clearer.

Aqueous alteration products have been documented in CI, CM, CV, CO and CR chondrites, and can include phases such as fayalite, serpentines, tochilinite, and others (Brearley, 2006). Detailed thermodynamic analysis of aqueous alteration in CI, CM, CV, CO and CR chondrites (Zolensky et al., 1989; Bourcier and Zolensky, 1992; Zolensky et al., 1993) shows that these phases can be produced by interaction with fluids at low temperatures and oxygen fugacities as high as IW+2.6. More focused studies of fayalite formation (Zolotov et al., 2006) show that it can occur across a range of conditions from T = 50 °C, P=10.1 bar, log (fH_2/fH_2O) = 3 to 4, which corresponds to log fO_2 = -79.3 to -81.3, to T = 150 °C, P=104.8 bar, log (fH_2/fH_2O) = 2 to 3, which corresponds to log fO_2 = -61.02 to -59.02. The latter conditions correspond to IW-1.3 to IW-3.3. It is clear that aqueous alteration can produce fayalite at fO_2 conditions equivalent to those experienced during chondrule-formation and even the transient oxidizing environment experienced by CAIs, but formation of some phases, such as smectite, saponite, phyllosilicates, and magnetite, requires more oxidizing conditions, above the IW buffer.

Achondrites

Our new measurements provide fO_2 estimates for several achondrite groups for which traditional barometry is not possible, and these are compared to previous measurements and calculations for achondrite groups (Fig. 6). The most reduced achondrites are the aubrites, which contain nearly FeO-free silicates and FeNi metal that has wt% levels of Si (e.g., Fogel, 2005). Silicate inclusions in some iron meteorites allow use of various redox equilibria to constrain oxygen fugacity. The IAB, IIICD, and IIE irons yield fO_2s ranging from IW-4 to IW-2.2 (Fig. 6). Work on other iron groups examining the significance of accessory phases such as chromite, phosphides and silica show that they formed over a range of fO_2 perhaps wider than that defined by the silicate-bearing irons in Figure 6 (Isa et al., 2015). Acapulcoites/lodranites and winonaites record fO_2s between IW-3 and IW-1.5 (this study; Benedix et al., 2005), while ureilites show a slightly wider range, from IW-3.25 to IW-1.5 (Goodrich et al., 2013). Our results from diogenites and those provided by Stolper (1977) from experiments show that the HEDs likely formed at fO_2 conditions between IW-1.75 and IW-0.5 (Fig. 6). Based on electrochemical measurements and redox equilibria, main group pallasites equilibrated between IW-0.5 and IW-1 (Righter et al., 1990; this study). Brachinites and the GRA 06128/9 ungrouped achondrites record formation at IW and IW-0.5, respectively, based on our XANES measurements. Finally, angrites exhibit the most oxidized values for achondrites, with equilibration above the IW buffer at IW+1 (McKay et al., 1994; Jurewicz et al., 1993). Altogether, these groups define a range of 8 log fO_2 units and exhibit nearly continuous variation from the reduced aubrites to the most oxidized angrites (Figure 6). Achondrites span the same range as the primitive materials discussed in the previous section (CAIs, chondrules, matrix, dust; Fig. 5), showing that the same redox conditions were present whether materials were differentiated or undifferentiated.

Planets

Our knowledge of redox variations within Earth comes from direct samples of the mantle such as peridotite xenoliths and massif terranes, as well as mantle melts, such as mid ocean ridge, ocean island, and island arc basalts. As a result, we have a very detailed understanding of the variation of oxygen fugacity in Earth's upper mantle (Figure 7). For Mars and Moon, we have no direct samples of the mantle, but there are important constraints from basaltic and cumulate meteorites that originated from the surface or shallow crust of Mars (shergottites, nakhlites, ALH 84001), and lunar basalts and volcanic glasses. We have not recognized meteorites from Venus or Mercury, so constraints are fewer, but the recent MESSENGER mission provided new information for Mercury. Spectroscopy studies showed low FeO contents at the surface of Mercury (Emery et al., 1998), and coupled with the knowledge of a large metallic core (e.g., Goettel, 1988), indicates that Mercury may be very reduced. There have been limited experimental studies of very FeO-poor materials such as enstatite chondrites (Berthet et al., 2009; McCoy et al. 1999), but these, combined with newer studies influenced by MESSENGER results, are reinforcing the idea that Mercury may have differentiated under reduced conditions of IW-4 to IW-5. The similar FeO contents of surficial basalts to terrestrial basalts, and the similarly-sized Fe metallic cores of Venus and Earth, suggests an overall oxygen fugacity for the Venusian interior that is similar to that of Earth. The lack of an O-rich atmosphere and limited recycling via terrestrial-style tectonics means interaction between mantle, crust and atmosphere has likely been much less, and this may have limited the variation in fO_2 within Venus. However, Venus has been resurfaced in recent geologic time (e.g., Basilevsky et al., 1997) and that may allow chemical reaction between mantle and surface reservoirs. In addition, there may be a variation pro-

duced by high pressure processes and dissolution of volatiles (possibly different from Earth due to the high pressure, CO_2-rich atmosphere) in magmas.

Comparative planetology lessons from Earth reveal a multitude of processes operating at a planetary scale that can have a large influence on the oxygen fugacity. For example, planets hold more internal energy than small bodies, and therefore heating and melting processes have occurred over a more extended time period (even to present-day) and to great depths. As a result, magmas in planets ascend from greater depths than those in smaller, asteroid sized bodies. The decompression of a silicate melt upon ascent from the mantle can lead to a change in its $Fe^{3+}/\Sigma Fe$ ratio. This is a strong effect in the Earth (Kress and Carmichael, 1991), but is more subtle for Mars due to the properties of FeO-rich melts (Righter et al., 2013). Also linked to pressure is the enhanced solubility of volatiles at higher pressures. Terrestrial magmas are known to have appreciable H_2O, CO_2 and SO_2 contents (Holloway and Blank, 1994; Carroll and Webster, 1994), and Mars' wide fO_2 range is due to the influence of volatiles such as S_2, H_2O, and CO_2 (McCubbin et al., 2010; Righter et al., 2008a, 2009). High solubility at crustal pressures allows magmas to be volatile-bearing and, upon ascent, degassing leads to fO_2 variations at the surface. For example, S_2 loss can lead to reduction, as seen in nakhlites (Fig. 7), whereas later Cl loss can lead to oxidation (Righter et al., 2014; Fig. 7). Mercury may contain more reduced species, although the level of understanding for Mercury is currently primitive.

Shallow-level processes on planets, such as may occur in a magma chamber, include fractionation, degassing, and assimilation. Closed system fractionation of a basaltic magma can produce differentiated liquids that also contain more Fe^{3+} their parent liquids. Such processes have been documented in terrestrial magmas (Kelley and Cottrell, 2012) as well as martian magmas (Peslier et al., 2010). Degassing of dissolved volatile species can lead to changes in Fe

redox state in the magma (S_2, H_2O, Cl; although see Crabtree and Lange, 2012, for discussion), and finally, assimilation of surrounding rocks by a magma can lead to changes in the Fe redox state of the magma (e.g., oxidized crust or reduced crust compared to magma). Spectacular examples of the latter are the metal-bearing basalts in Germany and in Greenland (Disko Island), where assimilation of C-bearing sediment led to reduction and even the precipitation of metal (Bird et al., 1981). Concomitantly, assimilation of oxidized rocks can lead to oxidation of the intruding magma as well (Ague and Brimhall, 1988).

A final process documented in terrestrial settings is metasomatism. Deep lithospheric settings as well as the shallow, sub-arc mantle have been proposed as areas (among others) where mobile fluids have interacted with relatively dry mantle to cause metasomatism that can produce oxidized and volatile-bearing assemblages (mica-amphibole-rutile-ilmenite-diamond, or MARID, assemblages; Zhao et al., 1999). Such metasomatic processes have been considered for Mars and even the Moon (Treiman, 2003; Elardo et al., 2012).

When all these processes are accounted for and considered, mantle redox state can be assessed. For Earth, mantle and magmatic samples that have not been influenced by these processes yield a narrow range of fO_2, from IW+1 to IW+2 (Frost and McCammon, 2008). Some deeper parts of the mantle may be more reduced (Woodland and Koch, 2003), prompting some to propose that the lower mantle may be metal-saturated (Rohrbach et al., 2007). For Mars, there are two samples that may represent primitive mantle melts, Yamato 980459 and NWA 5789, and these require a mantle source region that was near IW to IW+1 (McKay et al., 2004; Shearer et al., 2006b; Herd, 2008; Gross et al., 2011). Samples from both Earth and Mars have been oxidized to values higher than initially present in their source mantle by ascent, fractionation, degassing, and assimilation. Although the origin of the Moon is likely linked to Earth through a

giant impact, lunar samples are more reduced than terrestrial peridotite and basalt. XANES studies of lunar glasses (Karner et al., 2006; Sutton et al., 2005), carbon solubility studies of lunar glasses (Nicholis and Rutherford, 2009; Weitz et al., 1997), and electrochemical studies of lunar basalt (Sato et al., 1973) all yield values of fO_2 between IW-0.5 and IW-2 (Figure 7). Some variability can be attributed to degassing and volatile solubilities, but overall the oxygen fugacity of the lunar mantle and basalt source regions is well-defined and relatively narrow. For Venus, we can assume processes and mantle domains with an overall similarity to Earth due to its moderate FeO contents, similar core size, and some evidence for alkaline basalts at the surface (Treiman, 2007). For Mercury, the ground-based observations and MESSENGER mission data has led to the general interpretation that Mercury is reduced and its mantle could be at IW-5 or IW-6 (Figure 7).

Cause of variation in fO_2

a) Nebular chemistry and transport

The fO_2 range defined by nebular or primitive materials starts at low fO_2 (near IW-6), as evident in solar nebular gas C/O ratios (Allende Prieto et al., 2002) as well as CAIs, enstatite chondrites, and some chondrules (Fig. 5). Higher fO_2s in primitive materials are also recorded by inclusions in CM2 chondrites, CAIs, FeO-bearing chondrules, and matrices in a wide range of chondrites, and range up to near the IW buffer. Because most of these objects are ancient, and formed within the first 5 Ma of solar system inception, it is clear that fO_2 variations were significant in the nebula. Evidence from meteorites and cometary (Stardust) materials also indicate that some of these objects record a wide range of fO_2, implying transport of material large distances within nebula. Variations in fO_2 in the solar system may arise from physical or chemical

factors, or both. For example, there could have been both vertical and radial transport in the solar nebula and both may have contributed to mobility of materials in the early solar system (e.g. Grossman et al., 2008). The nebula was likely heterogeneous initially, so chemical variation, such as in C/O ratios (Allende Prieto et al., 2002) or the relative proportions of H, C, and O in the solar nebula could have varied and contributed to fO_2 variation. The solar ratio of dust to gas in the nebula cannot produce FeO-bearing olivines, but increasing this ratio to 100x to 300x solar values results in a larger stability field for fayalite in condensing olivine (Grossman et al., 2008). Tenner et al. (2015) document a correlation between $\Delta^{17}O$ and olivine Mg# in chondrules from CR3 chondrites, and explain the variation with chondrule-melt equilibria involving dust enrichments of 100-200x for Type I chondrules and 2500x for Type II chondrules; they further speculate that the early Type I chondrules may have been produced in a dry environment, whereas the later, oxidized chondrules formed in a water-bearing environment (see also Grossman and Fedkin, 2015). Finally, Clayton (2005) argued that photo-dissociation of CO could have created a more oxidizing environment in the solar nebula. This idea gained some support from measurements of the composition of solar oxygen from the Genesis mission (McKeegan et al., 2011). It is fair to say that the chemical environment of the solar nebula, and its spatial heterogeneity, are fields of intense study and many questions remain unanswered.

b) Planetesimal formation (heat and fluids and impacts)

The range of fO_2 defined by achondrites is nearly the same as that in primitive materials, suggesting that the heating processes that formed the achondrites through melting and accumulation did not alter the fO_2 substantially, with an overall range of approximately IW-6 to IW. Aqueous alteration, on the other hand, has affected most carbonaceous chondrites (CI, CM, CV, CR, CK; Brearley, 2006) and is associated with oxidation. Although some alteration does not

require high fO_2 (e.g., production of fayalite), some phase equilibria suggest IW+3 to IW+7 at low temperatures. Similarly, CK chondrites show evidence for oxidation (exsolution lamellae of FeTi oxides; Righter and Neff, 2007), and V XANES data reported here indicate fO_2s as high as IW+3.5 to IW+6. Fluids may have been Cl-bearing (Cl-phosphates) and oxidized, but not necessarily water-rich. These results indicate that, in some asteroids, oxidation can produce materials locally with oxidized values outside the range defined by primitive materials. Studies of matrix and some fine grained dust particles also record high $Fe^{3+}/\Sigma Fe$ values (LeGuillou et al., 2015; Ogliore et al., 2010; Stodolna et al., 2013), consistent with oxidation above IW, but specific values are not yet defined.

c) Planet building: building blocks and planetary processes

Some terrestrial samples exhibit values as high as IW+8, and some Mars samples IW+3.5 to 4 (Fig. 7), and both can be explained by roles for tectonics, pressure, and volatile abundances and speciation, which are typically not as relevant or influential for asteroids and smaller bodies. In the case of Earth, mantle and crustal melting occurs at pressures between 8 and 0 GPa, and the high pressures allow for dissolution of significant volatile species such as H_2O, CO_2, SO_2, and H_2S into melts. Upon decompression and degassing, the redox state of a magma can become more oxidized or reduced, depending on which species are lost and the overall composition of the magma. Tectonics can also provide opportunities for oxidation. Although island arc basalts may show evidence for slightly greater fO_2 than ocean basin (MORB, OIB) basalts, the sub-arc mantle can be oxidized by fluid release from subducted slabs. The fluids react with overlying mantle to cause metasomatism or form oxidized peridotite. Some sub-arc mantle has been documented with evidence for equilibration at fO_2 values as high as IW+7 (McInnes et al., 1994). On Mars, polybaric melting, ascent and degassing of CO_2-rich melts can produce melts with a

wide range of fO_2, from IW to IW+3, and additional fractionation and degassing in shallow magma bodies can produce both oxidation and reduction, with the former up to IW+4 to 5 (e.g., Righter et al., 2008; Peslier et al., 2010; Righter et al., 2014).

The potential for pressure and volatile loss to widen the range of fO_2 recorded in planetary materials is significant, and such effects must be accounted for when comparing planetary materials to meteoritic or nebular samples. Additionally, the fO_2 conditions of core formation for Mars, Earth and Vesta (EPB) are consistently lower than that defined by mantle and basalt samples from these bodies. The disparity between conditions for terrestrial core formation and basalt production is clearly evident in Figure 7, whereas for Mars and Vesta it is more subtle. Core formation in Mars is thought to have occurred near IW-1.5, whereas the most reduced shergottites are near IW. Similarly, core formation modelling for siderophile elements in Vesta show conditions near IW-2, yet eucrites, diogenites, and possibly related pallasites all exhibit higher fO_2 near IW-1 or IW-1.5 (Fig. 6). Overall, there must be some oxidation during melting and ascent of magmas on these three bodies. When all secondary processes are considered (ascent, volatile exsolution, degassing), and fO_2 is defined for those samples unaffected by volatiles or degassing, the range of fO_2 of planetary mantles is IW-6 (Mercury) to IW-2 to IW-1.5 (Earth), to IW-1 to IW (Mars). This range is similar to that defined by primitive materials and achondrites. Implications are that a significant oxidized reservoir (>IW) was likely not present in the solar system available for planet building. Even though such high values are encountered in asteroidal materials, they did not apparently have a large influence on outcomes.

Finally, the planets grew by large impacts between differentiated proto-planets. This process has been modelled as merging of two bodies, usually with differing mantle FeO content (and thus oxygen fugacity), creating a new body with a new oxidation state. Fischer and Ciesla

(2014) have shown that, in some cases, FeO contents of the Earth-sized planets created in these simulations increase with time. However, when large impacts occur, an oxidized impactor does not necessarily cause oxidation of a more reduced target body. This has been assumed in the modelling done, perhaps due to the simplified chemical systems being considered, but a more realistic situation is that a more massive, reduced body will convert some of the oxidized material to a more reduced state. The modelling should also consider silicate liquids and high P-T conditions, since most proto-planets were likely at least partially molten, and would be again during and after the impact. The oxidation of the target body may be negligible, rather than incremental as frequently modelled (Bond et al., 2010; Fischer and Ciesla, 2014). The Fe redox equilibria in such major impacts must be modelled more realistically to know whether bodies in the last stages of accretion can become more oxidized, more reduced, or stay constant during planet building.

Summary and Future

There are many new techniques that can be applied to astromaterials to determine the redox state of elements and to determine oxygen fugacity. Electron energy loss spectroscopy (EELS) and x-ray absorption spectroscopy (XANES and EXAFS) both offer high spatial and energy resolution measurements that have just begun to be applied to natural samples. The focus of this study – redox state of V in spinels – has been carried out at relatively high fO_2 conditions, but could be quantified for low-fO_2 samples of IW-3 and below. Our results imply that there may be substantial V^{2+} in spinels formed at low fO_2s. However, the vanadium valence calibration for spinel at these very low pre-edge peak intensities may not be well-constrained. As the pre-edge peak intensity decreases going from V^{3+} to V^{2+}, there should be an accompanying energy shift to

lower energies in the main edge region and the main edge spectral shape should change to some extent. For example, comparing VO and V_2O_3 in Wong et al. (1984), the main edge shifts by about 1 eV. Energy shifts of that magnitude were not observed for spinels in the current study, and the main edge regions of all spectra are pretty similar to each other. Spinel may behave differently in this regard compared to other oxides. It is possible that the relation between pre-edge peak intensity, octahedral site asymmetry, and disordering is not well understood yet at reducing conditions. It seems there are some important issues to resolve and explore for application of V XANES to spinels equilibrated at low fO_2 (< IW-3). Finally, many measurements of $Fe^{3+}/\Sigma Fe$ on dust, reduced glasses, matrix and amorphous materials have not been correlated with oxygen fugacity in a quantitative way, only qualitatively. Quantitation will allow more direct comparisons between astromaterials collections and types of samples and could enhance our understanding of more primitive solar system materials.

The oxygen fugacity record in primitive materials, chondrites, achondrites and planets spans a wide range of fO_2 from IW-8 to IW+8, 16 orders of magnitude. The range within each group is similar and largely between IW-8 and IW+2, with the exception of Earth and Mars and a few oxidized chondrites. Earth exhibits the most oxidized mantle and magmas, presumably due to the influence of an O_2-rich atmosphere, liquid water oceans at the surface, and a hydrated deep interior. Mars is slightly oxidized, but its range is much more restricted than Earth's, suggesting a lesser or less-widespread role for water and oxygen in the magmatic evolution of the planet, consistent with its O-poor atmosphere and lack of oceans or large water masses (water is not unknown on Mars, just of lesser abundance relative to Earth; Villanueva et al., 2015). Of course, this assessment may need to be revised when Mars is more thoroughly sampled. Simulations of planet formation currently show Earth-like planets becoming more FeO-rich during ac-

cretion, but the simplified chemical systems considered may yield different results than multi-component, volatile-bearing, more realistic systems; this should be pursued in future modeling efforts.

Overall, we currently enjoy access to samples from a wide range of near-Earth objects, Moon, Mars, a Jupiter Family comet (Wild 2), solar wind, and cosmic dust. Although this is a broad range of materials, there are sampling gaps that will be addressed in future missions. OSIRIS-REx will launch in 2016 and return as much as 2 kg of carbonaceous asteroid material from Bennu in September 2023 (Lauretta et al., 2015). Hayabusa 2 launched in 2014 and will return samples of carbonaceous asteroid 162173 Ryugu in December 2020 (Tsuda et al., 2013). Comet sample return and lunar sample return have been featured as top prospects for sample return missions for the Discovery and New Frontiers programs. Technically challenging sample return missions to Venus and Mercury, or identification of venusian or mercurian meteorites among world collections, would revolutionize our understanding of planet formation in our and other solar systems. New samples from any or all of these bodies would help to elucidate the range of fO_2 recorded in astromaterials and ultimately better constrain the origin of our solar system.

Acknowledgements

This work was supported by an RTOP from the NASA Cosmochemistry / Emerging Worlds programs. Portions of this work were performed at GeoSoilEnviroCARS (Sector 13), Advanced Photon Source (APS), Argonne National Laboratory. GeoSoilEnviroCARS is supported by the National Science Foundation - Earth Sciences (EAR-1128799) and Department of Energy- GeoSciences (DE-FG02-94ER14466). This research used resources of the Advanced

Photon Source, a U.S. Department of Energy (DOE) Office of Science User Facility operated for the DOE Office of Science by Argonne National Laboratory under Contract No. DE-AC02-06CH11357. All meteorite samples were provided by the Meteorite Working Group except for the acapulcoites/lodranites (J. Herrin), GRA 06128 (A. Treiman), and ALH 84001 (M. Righter). The manuscript benefitted from the careful reviews and constructive comments of P. Burger, J. Paque, and AE S. Simon. We thank K. Putirka for the invitation to contribute a paper in celebration of the Mineralogical Society of America centennial, and KR wishes to acknowledge the enormous and continuing influence the society has had on his science and understanding of the natural world.

References:

Ague, J.J., and Brimhall, G.H. (1988) Magmatic arc asymmetry and distribution of anomalous plutonic belts in the batholiths of California: Effects of assimilation, crustal thickness, and depth of crystallization. Geological Society of America Bulletin, 100, 912-927.

Allende Prieto, C., Asplund, M., and Lambert, D.L. (2002) A reappraisal of the solar photospheric C/O ratio. Astrophysical Journal, 573, L137-L140.

Ash, R.D., Day, J.M.D., McDonough, W.F., Bellucci, J., Rumble, D., Liu, Y., and Taylor, L.A. (2008) Petrogenesis of the differentiated achondrite GRA 06129: trace elements and chronology. Lunar and Planetary Science Conference, 39, abstract #2271.

Basilevsky, A.T., Head, J.W., Schaber, G.G., Strom, R.G. (1997) The Resurfacing History of Venus. In S.W. Bougher, D.M. Hunten, and R.J. Philips, eds, "Venus II : Geology, Geophysics, Atmosphere, and Solar Wind Environment". Tucson, AZ : University of Arizona Press, 1047-1083.

Bassett, W.A., and Brown Jr, G.E. (1990) Synchrotron radiation-Applications in the earth sciences. Annual Review of Earth and Planetary Sciences, 18, 387-447.

Bell, A.S., Burger, P.V., Le, L., Shearer, C.K., Papike, J.J., Sutton, S.R., and Jones, J.H. (2014) XANES measurements of Cr valence in olivine and their applications to planetary basalts. American Mineralogist, 99, 1404-1412.

Benedix, G.K., Lauretta, D.S., and McCoy, T.J. (2005) Thermodynamic constraints on the formation conditions of winonaites and silicate-bearing IAB irons. Geochimica et Cosmochimica Acta, 69, 5123-5131.

Berthet, S., Malavergne, V., and Righter, K. (2009) Melting of the Indarch meteorite (EH4 chondrite) at 1GPa and variable oxygen fugacity: Implications for early planetary differentiation processes. Geochimica et Cosmochimica Acta, 73, 6402-6420.

Bird, J.M., Goodrich, C.A., and Weathers, M.S. (1981) Petrogenesis of Uivfaq iron, Disko Island, Greenland. Journal of Geophysical Research: Solid Earth, 86, 11787-11805.

Bischoff, A., Vogel, N., and Roszjar, J. (2011) The Rumuruti chondrite group. Chemie der Erde-Geochemistry, 71, 101-133.

Bond, J.C., Lauretta, D.S., and O'Brien, D.P. (2010) Making the Earth: Combining dynamics and chemistry in the Solar System. Icarus, 205, 321-337.

Bourcier, W.L., and Zolensky, M.E. (1992) Computer modeling of aqueous alteration on carbonaceous chondrite parent bodies. Lunar and Planetary Science Conference, 23, 143-144.

Bradley, J. P. (1994) Nanometer-scale mineralogy and petrography of fine-grained aggregates in anhydrous interplanetary dust particles. Geochimica et Cosmochimica Acta 58, 2123-2134.

Brearley, A.J. (2006) The action of water. *Meteorites and the early solar system II*, *1*, 584-624.

Campbell A. J., Humayun M. and Weisberg M. K. (2002) Siderophile element constraints on the formation of metal in the metal-rich chondrites Bencubbin, Weatherford, and Gujba. Geochimica et Cosmochimica Acta 66, 647–660.

Carmichael, I.S.E. (1966) The iron-titanium oxides of salic volcanic rocks and their associated ferromagnesian silicates. Contributions to Mineralogy and Petrology, 14, 36-64.

Carmichael, I.S.E. (1991) The redox states of basic and silicic magmas: a reflection of their source regions?. Contributions to Mineralogy and Petrology, 106, 129-141.

Carmichael, I.S.E., and Ghiorso, M.S. (1990) The effect of oxygen fugacity on the redox state of natural liquids and their crystallizing phases. Reviews in Mineralogy and Geochemistry, 24, 191-212.

Carroll, M.R., and Webster, J.D. (1994) Solubilities of sulfur, noble gases, nitrogen, chlorine, and fluorine in magmas. Reviews in Mineralogy and Geochemistry, 30, 231-279.

Chase, M.W. (1986) JANAF thermochemical tables. JANAF thermochemical tables, by Chase, MW Washington, DC: American Chemical Society; New York: American Institute of Physics for the National Bureau of Standards, United States. National Bureau of Standards., 1.

Clayton, R.N. (2005) 1.06: Oxygen Isotopes in Meteorites. *Meteorites, Comets, and Planets: Treatise on Geochemistry*, *1*, 129.

Connolly, H.C., Hewins, R.H., Ash, R.D., Zanda, B., Lofgren, G.E., and Bourot-Denise, M. (1994) Carbon and the formation of reduced chondrules. Nature, 371, 136-139.

Crabtree, S.M., and Lange, R.A. (2012) An evaluation of the effect of degassing on the oxidation state of hydrous andesite and dacite magmas: a comparison of pre-and post-eruptive Fe^{2+} concentrations. Contributions to Mineralogy and Petrology, 163, 209-224.

Danielson, L.R., Righter, K., and Humayun, M. (2009) Trace element chemistry of Cumulus Ridge 04071 pallasite with implications for main group pallasites. Meteoritics and Planetary Science, 44, 1019-1032.

Dowty, E., Clark, J.R. (1973) Crystal structure refinement and optical properties of a Ti^{3+} fassaite from the Allende meteorite. American Mineralogist, 58, 230–242.

Dyar, M.D., Gunter, M.E., Delaney, J.S., Lanzarotti, A., and Sutton, S.R. (2002) Systematics in the structure and XANES spectra of pyroxenes, amphiboles, and micas as derived from oriented single crystals. The Canadian Mineralogist, 40, 1375-1393.

Dyl, K.A., Simon, J.I., and Young, E.D. (2011) Valence state of titanium in the Wark–Lovering rim of a Leoville CAI as a record of progressive oxidation in the early Solar Nebula. Geochimica et Cosmochimica Acta, 75, 937-949.

Elardo, S.M., McCubbin, F.M., and Shearer, C.K. (2012) Chromite symplectites in Mg-suite troctolite 76535 as evidence for infiltration metasomatism of a lunar layered intrusion. Geochimica et Cosmochimica Acta, 87, 154-177.

Emery, J. P., Sprague, A. L., Witteborn, F. C., Colwell, J. E., Kozlowski, R. W. H., and Wooden, D. H. (1998) Mercury: Thermal modeling and mid-infrared (5–12 μm) observations. Icarus, 136, 104-123.

Fedkin, A. V., Grossman, L., Humayun, M., Simon, S.B., Campbell, A.J. (2015) Condensates from vapor made by impacts between metal-, silicate-rich bodies: Comparison with metal and chondrules in CB chondrites. Geochimica et Cosmochimica Acta 164, 236-261.

Fischer, R.A., and Ciesla, F.J. (2014) Dynamics of the terrestrial planets from a large number of N-body simulations. Earth and Planetary Science Letters, 392, 28-38.

Fogel, R.A. (2005) Aubrite basalt vitrophyres: The missing basaltic component and high-sulfur silicate melts. Geochimica et Cosmochimica Acta, 69, 1633-1648.

Frost, B.R. (1991) Introduction to oxygen fugacity and its petrologic importance. Reviews in Mineralogy and Geochemistry, 25, 1-9.

Frost, D.J., and McCammon, C.A. (2008) The redox state of Earth's mantle. Annual Reviews of Earth and Planetary Science, 36, 389-420.

Gainsforth, Z., Butterworth, A.L., Stodolna, J., Westphal, A.J., Huss, G.R., Nagashima, K., and Simionovici, A.S. (2015) Constraints on the formation environment of two chondrule-like igneous particles from comet 81P/Wild 2. Meteoritics and Planetary Science, 50, 976-1004.

Garvie, L.A., and Buseck, P.R. (1998) Ratios of ferrous to ferric iron from nanometre-sized areas in minerals. Nature, 396, 667-670.

Goettel, K. A. (1988) Present bounds on the bulk composition of Mercury: Implications for planetary formation processes. *Mercury*, eds. Vilas, F., Chapman, C.R., Matthews, M.S., Tucson, Arizona, University of Arizona Press, 613-621.

Goodrich, C.A., Sutton, S.R., Wirick, S., and Jercinovic, M.J. (2013) Chromium valences in ureilite olivine and implications for ureilite petrogenesis. Geochimica et Cosmochimica Acta, 122, 280-305.

Gross, J., Treiman, A.H., Filiberto, J., and Herd, C.D. (2011) Primitive olivine-phyric shergottite NWA 5789: Petrography, mineral chemistry, and cooling history imply a magma similar to Yamato-980459. Meteoritics and Planetary Science, 46, 116-133.

Grossman, L. and Fedkin, A.V. (2015) Dust Enrichment: Less than Meets the Eye. 78th Annual Meeting of the Meteoritical Society, held July 27-31, 2015 in Berkeley, California. LPI Contribution No. 1856, p.5126.

Grossman, L., Olsen, E., Lattimer, J.M. (1979) Silicon in carbonaceous chondrite metal: Relic of high-temperature condensation. Science, 206, 449–451.

Grossman, L., Beckett, J.R., Fedkin, A.V., Simon, S.B., and Ciesla, F.J. (2008) Redox conditions in the solar nebula: Observational, experimental, and theoretical constraints. Reviews in Mineralogy and Geochemistry, 68, 93-140.

Hanson, B., and Jones, J. H. (1998) The systematics of Cr^{3+} and Cr^{2+} partitioning between olivine and liquid in the presence of spinel. American Mineralogist, *83*, 669-684.

Herd C.D.K. (2008) Basalts as probes of planetary interior redox state. In Oxygen in the solar system, edited by MacPherson G., Reviews in Mineralogy and Geochemistry, 68, 527–553.

Herd, C.D., Papike, J.J., and Brearley, A.J. (2001) Oxygen fugacity of martian basalts from electron microprobe oxygen and TEM-EELS analyses of Fe-Ti oxides. American Mineralogist, 86, 1015-1024.

Hewins, R. H., & Ulmer, G. C. (1984) Intrinsic oxygen fugacities of diogenites and mesosiderite clasts. Geochimica et Cosmochimica Acta, 48, 1555-1560.

Hillgren, V.J., Gessmann, C.K., and Li, J. (2000) An experimental perspective on the light element in Earth's core. In R. Canup and K. Righter, eds., *Origin of the Earth and Moon*, University of Arizona Press, Tucson, Arizona, 245-263.

Holloway, J.R., and Blank, J.G. (1994) Application of experimental results to COH species in natural melts. Reviews in Mineralogy, 30, 187-187.

Ihinger, P.D., and Stolper, E. (1986) The color of meteoritic hibonite: an indicator of oxygen fugacity. Earth and Planetary Science Letters, 78, 67-79.

Isa, J., McKeegan, K.D., and Wasson, J.T. (2015) Study of Inclusions in Iron Meteorites, Cr-Bearing Sulfide Inclusions in IVA Iron Meteorites. Lunar and Planetary Science Conference, 46, abstract #3013.

Joswiak, D.J., Brownlee, D.E., Matrajt, G., Westphal, A.J., and Snead, C.J. (2009) Kosmochloric Ca-rich pyroxenes and FeO-rich olivines (Kool grains) and associated phases in Stardust tracks and chondritic porous interplanetary dust particles: Possible precursors to FeO-rich type II chondrules in ordinary chondrites. Meteoritics and Planetary Science, 44, 1561-1588.

Jurewicz, A.J.G., Mittlefehldt, D.W., and Jones, J.H. (1993) Experimental partial melting of the Allende (CV) and Murchison (CM) chondrites and the origin of asteroidal basalts. Geochimica et Cosmochimica Acta, 57, 2123-2139.

Kallemeyn, G.W., Rubin, A.E., and Wasson, J.T. (1991) The compositional classification of chondrites: V. The Karoonda (CK) group of carbonaceous chondrites. Geochimica et Cosmochimica Acta, 55, 881-892.

Karner, J.M., Sutton, S.R., Papike, J.J., Shearer, C.K., Jones, J.H., and Newville, M. (2006) Application of a new vanadium valence oxybarometer to basaltic glasses from the Earth, Moon, and Mars. American Mineralogist, 91, 270-277.

Keller, L.P., and Messenger, S. (2011) On the origins of GEMS grains. Geochimica et Cosmochimica Acta, 75, 5336-5365.

Kelley, K.A., and Cottrell, E. (2012) The influence of magmatic differentiation on the oxidation state of Fe in a basaltic arc magma. Earth and Planetary Science Letters, 329, 109-121.

Kersting, A.B., Arculus, R.J., Delano, J.W., and Loureiro, D. (1989) Electrochemical measurements bearing on the oxidation state of the Skaergaard Layered Intrusion. Contributions to Mineralogy and Petrology, 102, 376-388.

Kessel, R., Beckett, J.R., Huss, G.R., and Stolper, E.M. (2004) The activity of chromite in multi-component spinels: Implications for T- fO_2 conditions of equilibrated H chondrites. Meteoritics and Planetary Science, 39, 1287-1305.

Kozul, J.M., Ulmer, G.C., and Hewins, R.H. (1988) Intrinsic fugacity measurements of some Allende Type B inclusions. Geochimica et Cosmochimica Acta, 52, 2707-2716.

Kress, V.C., and Carmichael, I.S.E. (1991) The compressibility of silicate liquids containing Fe_2O_3 and the effect of composition, temperature, oxygen fugacity and pressure on their redox states. Contributions to Mineralogy and Petrology, 108, 82-92.

Lauretta, D.S., Bartels, A.E., Barucci, M.A., Bierhaus, E.B., Binzel, R.P., Bottke, W.F., ... and Walsh, K.J. (2015) The OSIRIS-REx target asteroid (101955) Bennu: Constraints on its physical, geological, and dynamical nature from astronomical observations. Meteoritics and Planetary Science, 50, 834-849.

Le Guillou, C., Changela, H.G., and Brearley, A.J. (2015) Widespread oxidized and hydrated amorphous silicates in CR chondrites matrices: Implications for alteration conditions and H 2 degassing of asteroids. Earth and Planetary Science Letters, 420, 162-173.

Lehner, S.W., Petaev, M.I., Zolotov, M.Y., and Buseck, P.R. (2013) Formation of niningerite by silicate sulfidation in EH3 enstatite chondrites. Geochimica et Cosmochimica Acta, 101, 34-56.

Leroux, H., Rietmeijer, F.J., Velbel, M.A., Brearley, A.J., Jacob, D., Langenhorst, F., ... and Zolensky, M.E. (2008) A TEM study of thermally modified comet 81P/Wild 2 dust particles by interactions with the aerogel matrix during the Stardust capture process. Meteoritics and Planetary Science, 43, 97-120.

Leroux, H., Roskosz, M., and Jacob, D. (2009) Oxidation state of iron and extensive redistribution of sulfur in thermally modified Stardust particles. Geochimica et Cosmochimica Acta, 73, 767-777.

Lusby, D., Scott, E.R.D., and Keil, K. (1987) Ubiquitous high-FeO silicates in enstatite chondrites. Journal of Geophysical Research: Solid Earth, 92, E679–E695.

McCoy, T. J., Keil, K., Clayton, R. N., Mayeda, T. K., Bogard, D. D., Garrison, D. H., and Wieler, R. (1997) A petrologic and isotopic study of lodranites: Evidence for early formation as partial melt residues from heterogeneous precursors. Geochimica et Cosmochimica Acta, 61, 623-637.

McCoy, T.J., Dickinson, T.L., and Lofgren, G.E. (1999) Partial melting of the Indarch (EH4) meteorite: A textural, chemical, and phase relations view of melting and melt migration. Meteoritics and Planetary Science, 34, 735-746.

McCubbin, F.M., Riner, M.A., Vander Kaaden, K.E., and Burkemper, L.K. (2012) Is Mercury a volatile-rich planet?. Geophysical Research Letters 39, 9.

McCubbin, F.M., Smirnov, A., Nekvasil, H., Wang, J., Hauri, E., and Lindsley, D.H. (2010) Hydrous magmatism on Mars: A source of water for the surface and subsurface during the Amazonian. Earth and Planetary Science Letters, 292, 132-138.

McInnes, B.I., and Cameron, E.M. (1994) Carbonated, alkaline hybridizing melts from a sub-arc environment: Mantle wedge samples from the Tabar-Lihir-Tanga-Feni arc, Papua New Guinea. Earth and Planetary Science Letters, 122, 125-141.

McKay, G., Le, L., Wagstaff, J., and Crozaz, G. (1994) Experimental partitioning of rare earth elements and strontium: Constraints on petrogenesis and redox conditions during crystalliza-

tion of Antarctic angrite Lewis Cliff 86010. Geochimica et Cosmochimica Acta, 58, 2911-2919.

McKay G., Le L., Schwandt C., Mikouchi T., Koizumi E., and Jones J.H. (2004) Yamato 980459: The most primitive shergottite? Lunar and Planetary Science Conference, 35, abstract #2154.

McKeegan, K.D., Kallio, A.P.A., Heber, V.S., Jarzebinski, G., Mao, P.H., Coath, C.D., ... and Burnett, D.S. (2011) The oxygen isotopic composition of the Sun inferred from captured solar wind. Science, 332, 1528-1532.

McKeown, D.A., Buechele, A.C., Tappero, R., McCoy, T.J., and Gardner-Vandy, K.G. (2014) X-ray absorption characterization of Cr in forsterite within the MacAlpine Hills 88136 EL3 chondritic meteorite. American Mineralogist, 99, 190-197.

Mittlefehldt, D. W., Lindstrom, M. M., Bogard, D. D., Garrison, D. H., and Field, S. W. (1996) Acapulco-and Lodran-like achondrites: Petrology, geochemistry, chronology, and origin. Geochimica et Cosmochimica Acta, 60, 867-882.

Nakamura, T., Noguchi, T., Tsuchiyama, A., Ushikubo, T., Kita, N. T., Valley, J.W., ... and Nakano, T. (2008) Chondrule-like objects in short-period comet 81P/Wild 2. Science, 321, 1664-1667.

Nicholis, M.G., and Rutherford, M.J. (2009) Graphite oxidation in the Apollo 17 orange glass magma: Implications for the generation of a lunar volcanic gas phase. Geochimica et Cosmochimica Acta, 73, 5905-5917.

Noguchi, T., Hicks, L.J., Bridges, J.C., Gurman, S.J., and Kimura, M. (2013) Comparing asteroid Itokawa samples to the Tuxtuac LL5 chondrite with X-ray absorption spectroscopy. Lunar and Planetary Science Conference, 44, abstract # 1147.

Ogliore, R.C., Butterworth, A.L., Fakra, S.C., Gainsforth, Z., Marcus, M.A., and Westphal, A.J. (2010) Comparison of the oxidation state of Fe in comet 81P/Wild 2 and chondritic-porous interplanetary dust particles. Earth and Planetary Science Letters, 296, 278-286.

Osborn, E.F. (1959) Role of oxygen pressure in the crystallization and differentiation of basaltic magma. American Journal of Science, 257, 609–647.

Palme H., Hutcheon I.D., and Spettel B. (1994) Composition and origin of refractory-metal-rich assemblages in a Ca, Al-rich Allende inclusion. Geochimica et Cosmochimica Acta, 58,495-513

Papike, J.J., Karner, J.M., and Shearer, C.K. (2004) Letter. Comparative planetary mineralogy: V/(Cr+ Al) systematics in chromite as an indicator of relative oxygen fugacity. American Mineralogist, 89, 1557-1560.

Papike, J.J., Burger, P.V., Bell, A.S., Le, L., Shearer, C.K., Sutton, S.R., ... and Newville, M. (2013) Letter. Developing vanadium valence state oxybarometers (spinel-melt, olivine-melt, spinel-olivine) and V/(Cr+Al) partitioning (spinel-melt) for martian olivine-phyric basalts. American Mineralogist, 98, 2193-2196.

Papike, J. J., Burger, P. V., Bell, A. S., Shearer, C., Le, L., and Jones, J. (2015) Normal to inverse transition in martian spinel: Understanding the interplay between chromium, vanadium, and iron valence state partitioning through a crystal-chemical lens. American Mineralogist, 100, 2018-2025.

Paque, J.M., Sutton, S.R., Simon, S.B., Beckett, J.R., Burnett, D.S., Grossman, L., ... and Connolly, H.C. (2013) XANES and Mg isotopic analyses of spinels in Ca-Al-rich inclusions: Evidence for formation under oxidizing conditions. Meteoritics and Planetary Science, 48, 2015-2043.

Peslier, A., Hnatyshin, D., Herd, C.D.K., Walton, E.L., Brandon, A.D., Lapen, T.J., and Shafer, J.T. (2010) Crystallization, melt inclusion, and redox history of a Martian meteorite: Olivine-phyric shergottite Larkman Nunatak 06319. Geochimica et Cosmochimica Acta, 74, 4543-4576.

Petaev, M.I., Wood, J.A., Meibom, A., Krot, A.N., and Keil, K. (2003) The ZONMET thermo-dynamic and kinetic model of metal condensation. Geochimica et Cosmochimica Acta, 67, 1737-1751.

Righter, K., and Drake, M.J. (1996) Core formation in Earth's moon, Mars, and Vesta. Icarus, 124, 513-529.

Righter, K., and Neff, K.E. (2007) Temperature and oxygen fugacity constraints on CK and R chondrites and implications for water and oxidation in the early solar system. Polar Science, 1, 25-44.

Righter, K., Arculus, R.J., Delano, J.W., and Paslick, C. (1990) Electrochemical measurements and thermodynamic calculations of redox equilibria in pallasite meteorites: Implications for the eucrite parent body. Geochimica et Cosmochimica Acta, 54, 1803-1815.

Righter, K., Sutton, S.R., Newville, M., Le, L., Schwandt, C.S., Uchida, H., and Downs, R.T. (2006a) An experimental study of the oxidation state of vanadium in spinel and basaltic melt with implications for the origin of planetary basalt. American Mineraogist, 91, 1643-1656.

Righter, K., Drake, M.J., and Scott, E. (2006b) Compositional relationships between meteorites and terrestrial planets. Meteorites and the early solar system II, 943, 803-828.

Righter, K., Yang, H., Costin, G., and Downs, R.T. (2008a) Oxygen fugacity in the Martian mantle controlled by carbon: New constraints from the nakhlite MIL 03346. Meteoritics & Planetary Science, 43, 1709-1723.

Righter, K., Chesley, J.T., Caiazza, C.M., Gibson, E.K., and Ruiz, J. (2008b) Re and Os concentrations in arc basalts: the roles of volatility and source region fO_2 variations. Geochimica et Cosmochimica Acta, 72, 926-947.

Righter, K., Pando, K., and Danielson, L.R. (2009) Experimental evidence for sulfur-rich martian magmas: Implications for volcanism and surficial sulfur sources. Earth and Planetary Science Letters, 288, 235-243.

Righter, K., Danielson, L.R., Pando, K., Morris, R.V., Graff, T.G., Agresti, D.G., and Lanzirotti, A. (2013) Redox systematics of martian magmas with implications for magnetite stability. American Mineralogist, 98, 616-628.

Righter, K., Keller, L.P., Rahman, Z., and Christoffersen, R. (2014) Redox-driven exsolution of iron-titanium oxides in magnetite in Miller Range (MIL) 03346 nakhlite: Evidence for post crystallization oxidation in the nakhlite cumulate pile?. American Mineralogist, 99, 2313-2319.

Robie, R.A., Hemmingway, B.S., and Fisher, J.R. (1978) Thermodynamic properties of minerals and related substances at 298.15 K and 1 bar pressure and at higher temperature. United States Geological Survey Bulletin 1452.

Rohrbach, A., Ballhaus, C., Golla–Schindler, U., Ulmer, P., Kamenetsky, V.S., and Kuzmin, D.V. (2007) Metal saturation in the upper mantle. Nature, 449, 456-458.

Rubin, A. E. (2007) Petrogenesis of acapulcoites and lodranites: A shock-melting model. Geochimica et Cosmochimica Acta 71, 2383-2401.

Sato, M., Hickling, N.L., and McLane, J.E. (1973) Oxygen fugacity values of Apollo 12, 14, and 15 lunar samples and reduced state of lunar magmas. Proceedings 4th Lunar and Planetary Science Conference, 1061-1070.

Schrader, D.L., Connolly, H.C., Lauretta, D.S., Nagashima, K., Huss, G.R., Davidson, J., and Domanik, K.J. (2013) The formation and alteration of the Renazzo-like carbonaceous chondrites II: linking O-isotope composition and oxidation state of chondrule olivine. Geochimica et Cosmochimica Acta, 101, 302-327.

Shearer, C.K., Papike, J.J., and Karner, J.M. (2006a) Pyroxene europium valence oxybarometer: Effects of pyroxene composition, melt composition, and crystallization kinetics. American Mineralogist, 91, 1565-1573.

Shearer C.K., McKay G., Papike J.J., and Karner J.M. (2006b) Valence state partitioning of vanadium between olivine-liquid: Estimates of the oxygen fugacity of Y980459 and application to other olivine-phyric martian basalts. American Mineralogist, 91, 1657–1663.

Shearer, C.K., Burger, P.V., Neal, C.R., Sharp, Z., Borg, L.E., Spivak-Birndorf, L., and Fernandes, V. A. (2008) Letter. A unique glimpse into asteroidal melting processes in the early solar system from the Graves Nunatak 06128/06129 achondrites. American Mineralogist, 93, 1937-1940.

Shearer, C. K., P. V. Burger, C. Neal, Z. Sharp, L. Spivak-Birndorf, L. Borg, V. A. Fernandes (2010) Non-basaltic asteroidal magmatism during the earliest stages of solar system evolution: A view from Antarctic achondrites Graves Nunatak 06128 and 06129. Geochimica et Cosmochimica Acta 74, 1172-1199.

Shock, E.L., Amend, J.P., and Zolotov, M.Y. (2000) The early Earth vs. the origin of life. In R. Canup and K. Righter, eds., *Origin of the Earth and Moon*, Univ. Arizona Press., Tucson, Arizona, 527-543.

Simon, J.I., Hutcheon, I.D., Simon, S.B., Matzel, J.E., Ramon, E.C., Weber, P.K., and DePaolo, D.J. (2011) Oxygen isotope variations at the margin of a CAI records circulation within the solar nebula. Science, 331, 1175-1178.

Simon, J.I., Young, E.D., Russell, S.S., Tonui, E.K., Dyl, K.A., and Manning, C.E. (2005) A short timescale for changing oxygen fugacity in the solar nebula revealed by high-resolution 26 Al–26 Mg dating of CAI rims. Earth and Planetary Science Letters, 238, 272-283.

Simon, S.B., Joswiak, D.J., Ishii, H.A., Bradley, J.P., Chi, M., Grossman, L., and McKeegan, K.D. (2008) A refractory inclusion returned by Stardust from comet 81P/Wild 2. Meteoritics and Planetary Science, 43, 1861-1877.

Simon, S.B., Sutton, S.R., and Grossman, L. (2007) Valence of titanium and vanadium in pyroxene in refractory inclusion interiors and rims. Geochimica et Cosmochimica Acta, 71, 3098-3118.

Simon, S. B., Sutton, S. R., & Grossman, L. (2011) The growing inventory of Ti^{3+}-bearing objects from the solar nebula. In Workshop on Formation of the First Solids in the solar system LPI Contribution 1639, abstract #9074.

Simon, S.B., Sutton, S.R., and Grossman, L. (2013) The Valence of Ti in Enstatite Chondrites: Not What you Might Think. Lunar and Planetary Science Conference, 44, abstract #2270.

Simon, S.B., Sutton, S.R., and Grossman, L. (2015) The Valence and Coordination of Ti in Olivine and Pyroxene in Ordinary and Enstatite Chondrites as a Function of Metamorphic Grade. Lunar and Planetary Science Conference, 46, abstract # 2141.

Stodolna, J., Gainsforth, Z., Leroux, H., Butterworth, A.L., Tyliszczak, T., Jacob, D., and Westphal, A.J. (2013) Iron valence state of fine-grained material from the Jupiter family

comet 81P/Wild 2–A coordinated TEM/STEM EDS/STXM study. Geochimica et Cosmochimica Acta, 122, 1-16.

Stolper, E. (1977) Experimental petrology of eucritic meteorites. Geochimica et Cosmochimica Acta, 41, 587-611.

Sutton, S.R., Karner, J., Papike, J., Delaney, J.S., Shearer, C., Newville, M., and Dyar, M.D. (2005) Vanadium K edge XANES of synthetic and natural basaltic glasses and application to microscale oxygen barometry. Geochimica et Cosmochimica Acta, 69, 2333-2348.

Tenner, T.J., Nakashima, D., Ushikubo, T., Kita, N. T., and Weisberg, M. K. (2015) Oxygen isotope ratios of FeO-poor chondrules in CR3 chondrites: influence of dust enrichment and H_2O during chondrule formation. Geochimica et Cosmochimica Acta, 148, 228-250.

Trail, D., Watson, E.B., and Tailby, N.D. (2011) The oxidation state of Hadean magmas and implications for early Earth/'s atmosphere. Nature, 480, 79-82.

Treiman, A.H. (2003) Chemical compositions of martian basalts (shergottites): Some inferences on basalt formation, mantle metasomatism, and differentiation in Mars. Meteoritics and Planetary Science, 38, 1849-1864.

Treiman, A.H. (2007) Geochemistry of Venus' Surface: Current Limitations as Future Opportunities, in Exploring Venus as a Terrestrial Planet (eds L. W. Esposito, E. R. Stofan and T. E. Cravens), American Geophysical Union, Washington, D. C.. doi: 10.1029/176GM03.

Tsuda, Y., Yoshikawa, M., Abe, M., Minamino, H., and Nakazawa, S. (2013) System design of the hayabusa 2—asteroid sample return mission to 1999 ju3. Acta Astronautica, 91, 356-362.

Van Schmus, W.R., and Wood, J.A. (1967) A chemical-petrologic classification for the chondritic meteorites. Geochimica et Cosmochimica Acta, 31, 747-765.

Villanueva, G.L., Mumma, M.J., Novak, R.E., Käufl, H.U., Hartogh, P., Encrenaz, T., and Smith, M.D. (2015) Strong water isotopic anomalies in the martian atmosphere: Probing current and ancient reservoirs. Science, 348, 218-221.

Wadhwa, M. (2008) Redox conditions on small bodies, the Moon and Mars. Reviews in Mineralogy and Geochemistry 68, 493-510.

Weitz, C.M., Rutherford, M.J., and Head, J.W. (1997) Oxidation states and ascent history of the Apollo 17 volcanic beads as inferred from metal-glass equilibria. Geochimica et Cosmochimica Acta, 61, 2765-2775.

Westphal, A.J., Fakra, S.C., Gainsforth, Z., Marcus, M.A., Ogliore, R.C., and Butterworth, A.L. (2009) Mixing fraction of inner solar system material in Comet 81P/Wild2. The Astrophysical Journal, 694, 18.

Wong, J., Lytle, F.W., Messmer, R.P., and Maylotte, D.H. (1984) K-edge absorption spectra of selected vanadium compounds. Physical Review B, 30, 5596.

Woodland, A.B., and Koch, M. (2003) Variation in oxygen fugacity with depth in the upper mantle beneath the Kaapvaal craton, Southern Africa. Earth and Planetary Science Letters, 214, 295-310.

Xirouchakis, D., Draper, D.S., Schwandt, C.S., and Lanzirotti, A. (2002) Crystallization conditions of Los Angeles, a basaltic Martian meteorite. Geochimica et Cosmochimica Acta, 66, 1867-1880.

Zanda, B., Bourot-Denise, M., Perron, C., and Hewins, R.H. (1994) Origin and metamorphic redistribution of silicon, chromium, and phosphorus in the metal of chondrites. Science, 265, 1846-1849.

Zeigler R.A., Jolliff B., Korotev R.K., Rumble D. III, Carpenter P.K., and Wang A. (2008) Petrology, geochemistry, and likely provenance of unique achondrite Graves Nunataks 06128. Lunar and Planetary Science Conference, 39, abstract #2456.

Zhang, S., Livi, K.J., Gaillot, A.C., Stone, A.T., and Veblen, D.R. (2010) Determination of manganese valence states in (Mn^{3+}, Mn^{4+}) minerals by electron energy-loss spectroscopy. American Mineralogist, 95, 1741-1746.

Zhang, Y., Benoit, P.H., and Sears, D.W. (1995) The classification and complex thermal history of the enstatite chondrites. Journal of Geophysical Research: Planets, 100, 9417-9438.

Zhao, D., Essene, E.J., and Zhang, Y. (1999) An oxygen barometer for rutile–ilmenite assemblages: oxidation state of metasomatic agents in the mantle. Earth and Planetary Science Letters, 166, 127-137.

Zolensky, M. E., Bourcier, W. L., and Gooding, J. L. (1989) Aqueous alteration on the hydrous asteroids: Results of EQ3/6 computer simulations. Icarus, 78, 411-425.

Zolensky, M., Barrett, R., and Browning, L. (1993) Mineralogy and composition of matrix and chondrule rims in carbonaceous chondrites. Geochimica et Cosmochimica Acta, 57, 3123-3148.

Zolotov, M.Y., Mironenko, M.V., and Shock, E.L. (2006) Thermodynamic constraints on fayalite formation on parent bodies of chondrites. Meteoritics and Planetary Science, 41, 1775-1796.

Zolotov, M.Y., Sprague, A.L., Hauck, S.A., Nittler, L.R., Solomon, S.C., and Weider, S.Z. (2013) The redox state, FeO content, and origin of sulfur-rich magmas on Mercury. Journal of Geophysical Research: Planets, 118, 138-146.

Figure Captions

Figure 1: Chromite occurrences in various samples measured in this study. A) chromites (black grains indicated by yellow arrows) from the martian orthopyroxenite ALH 84001, transmitted light; b) chromites (yellow arrows) from the olivine-rich brachinite ALH 84025; transmitted light, crossed polarizers; c) Backscattered electron image of chromite enclosed by pentlandite, plagioclase and olivine in R chondrite LAP 04840; d) chromite inclusions (red arrows) in an olivine phenocryst from an olivine basalt (MGV-19) from the Mexican volcanic belt; transmitted light, crossed polarizers.

Figure 2: Correlation of V K pre-edge peak intensity with oxygen fugacity for spinels in the experiments of Righter et al. (2006a). A) Fit to data is of the form ΔIW = y0+a*(1-exp(-b*x))+c*(1-exp(-d*x)), with y0 = -8.6441, a = 11.6711, b=0.0360, c=14.0316, and d=0.0009. R = 0.9698, R^2 = 0.9404, and standard error of estimate is 0.78. B) Fit to the data in a more focused range, appropriate to the natural samples measured here; exponential fit with data between IW-1 and IW+4 (or pre-edge peak intensity between 0 and 100); standard error of estimate for this fit is 0.62.

Figure 3: V K pre-edge peak intensity for acapulcoites, lodranites, diogenites, brachinites, martian orthopyroxenite ALH 84001, two terrestrial basalts (MGV and SMT), and CK chondrites. FMQ refers to the fayalite-magnetite-quartz buffer. Arrows on the vertical axis show the pre-edge peak intensities corresponding to V3+/V2+ ratios of spinel and the FMQ buffer (IW is not shown but is near a pre-edge peak intensity value of 32), the former determined by a glass/spinel calibration (Righter et al., 2006a) and the latter determined by synthetic spinels as part of this work (Figure 2).

Figure 4: V K pre-edge peak intensity and Mg# in olivines from samples measured in this study. The variation in Mg# with oxidation is as expected in the metal-present field, with Mg# increasing as more FeO is reduced to Fe at fO_2 below IW. This trend reverses in the metal-free field above IW, as more FeO is oxidized to Fe_2O_3 at fO_2 above IW (Righter and Neff, 2007). The similarity of V oxidation state in GRA 06128 and brachinites, but different Mg# could be the result of differentiation processes.

Figure 5: Histogram of ΔIW values from various chondrites, components (CAI, chondrules, metal, matrix), and primitive materials from the literature. Solar values are from Allende Prieto et al. (2002), based on a C/O ratio of 0.5; CAI fassaite and CH metal are from Grossman et al. (2008) and Petaev et al. (2003), respectively. 'EL3 olivine' is based on XANES measurements of Cr in olivine by McKeown et al. (2014). Ranges of oxygen fugacity defined in refractory inclusions are from Ihinger and Stolper (1986), Paque et al. (2013) and Simon et al. (2007). Estimates for ordinary chondrites are from Ti valence (Simon et al., 2013) and metal-olivine-orthopyroxene equilibria (Righter and Drake, 1996; 112 H (blue), L (light blue), and LL samples (medium blue)). Constraints from chondrules are from Zanda et al. (1994) and Schrader et al. (2013). Estimates from Stardust (Inti, Iris, and Torajiro) and GEMS particles from Simon et al. (2008), Gainsforth et al. (2015), and data from Bradley (1994) and Keller and Messenger (2011). R chondrite estimates are from Righter and Neff (2007) and this study. All data and references used in this figure are summarized in Table S2. "Fassaite" refers to a Ti and Al-rich variety of clinopyroxene; Dowty and Clark, 1973.

Figure 6: Histograms of ΔIW values from this work (solid histograms; brachinites, GRA06128/129, pallasite CMS04071, diogenites, lodranites, and acapaulcoites) and values from previous work determined by experimental petrology (angrites; McKay et al., 1994; Jurewicz et

al., 1993), thermodynamic calculations (acapulcoites and winonaites, Righter and Drake, 1996; Benedix et al., 2005; silicate-bearing irons, Righter and Drake, 1996; aubrites, Righter et al., 2006; Fogel, 2005), electrochemical measurements (pallasites, Righter et al., 1990; diogenites, Hewins and Ulmer, 1984), and Cr XANES (ureilites, Goodrich et al., 2013). A complete listing of references for this figure is presented in Table S2.

Figure 7: Histograms of ΔIW values from planetary samples. Terrestrial samples (blues and greens) include continental xenoliths, abyssal peridotite, MORB, Kilauea basalt, andesites and lamprophyres from arcs all from Righter and Drake (1996). Mexican basalt samples are from this study. Martian samples (shades of red) include shergottite basalts from Righter and Drake (1996) as well as the range of oxidation recorded in cooling processes in shergottite LAR 06319 (Peslier et al., 2010), and the range of reduction recorded in nakhlite cumulates from Righter et al. (2014). ALH 84001 is from this study. Lunar samples (greys) include XANES studies of lunar glasses (Karner et al., 2006; Sutton et al., 2005), carbon solubility studies of lunar glasses (Nicholis and Rutherford, 2009; Weitz et al., 1997), and electrochemical studies of lunar basalt (Sato et al., 1973). Mercury samples are the range defined in studies by Zolotov et al. (2013) and McCubbin et al. (2012) based on low FeO and high S contents of the mercurian surface measured by MESSENGER. The range for Venus is a conservative estimate based on the size of its core, composition of surface basalts, but could be wider depending upon what planetary processes (volatile dissolution, degassing, and fractionation) may have operated on Venusian melts. The green and pink vertical bands represent the ΔIW thought to be associated with core formation in Earth and Mars, respectively. The vertical dashed line is the IW buffer, and the vertical dotted line at IW+2 represents the upper axis scale in the previous two plots illustrating the

relatively oxidized nature of terrestrial and martian samples. Complete listing of references in Table S2.

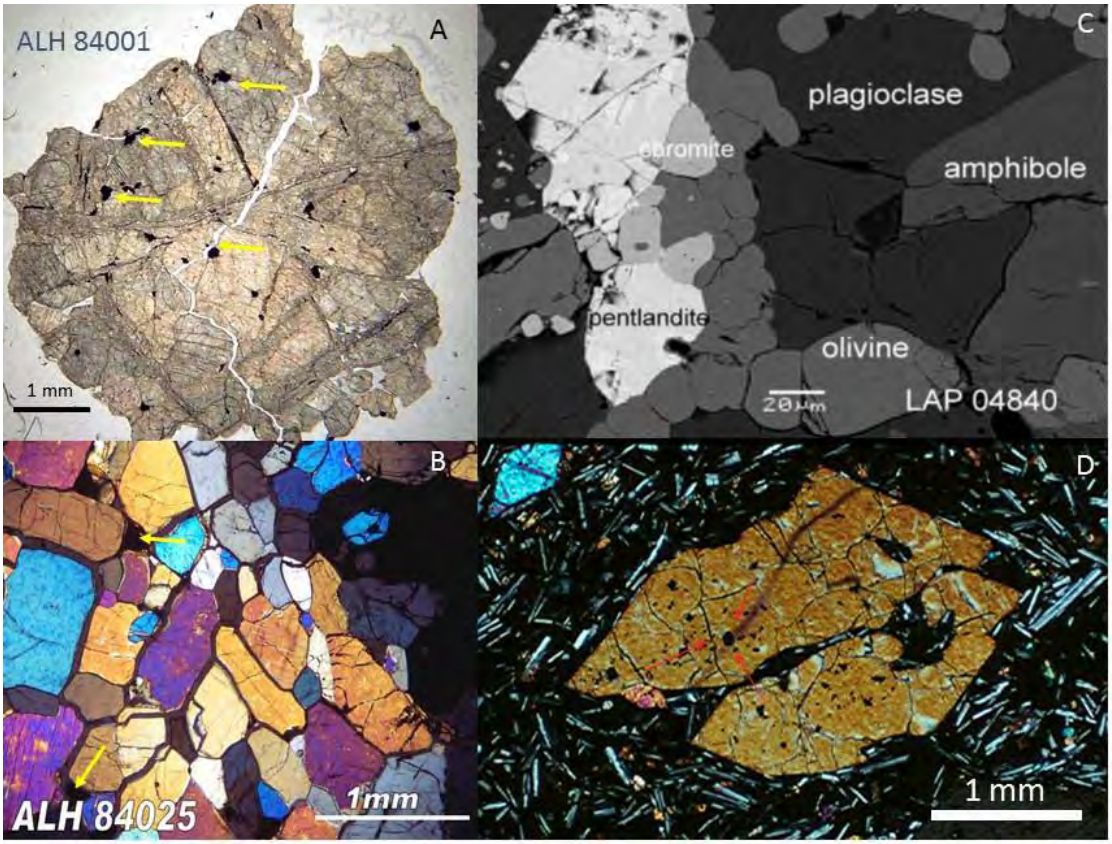

Figure 1

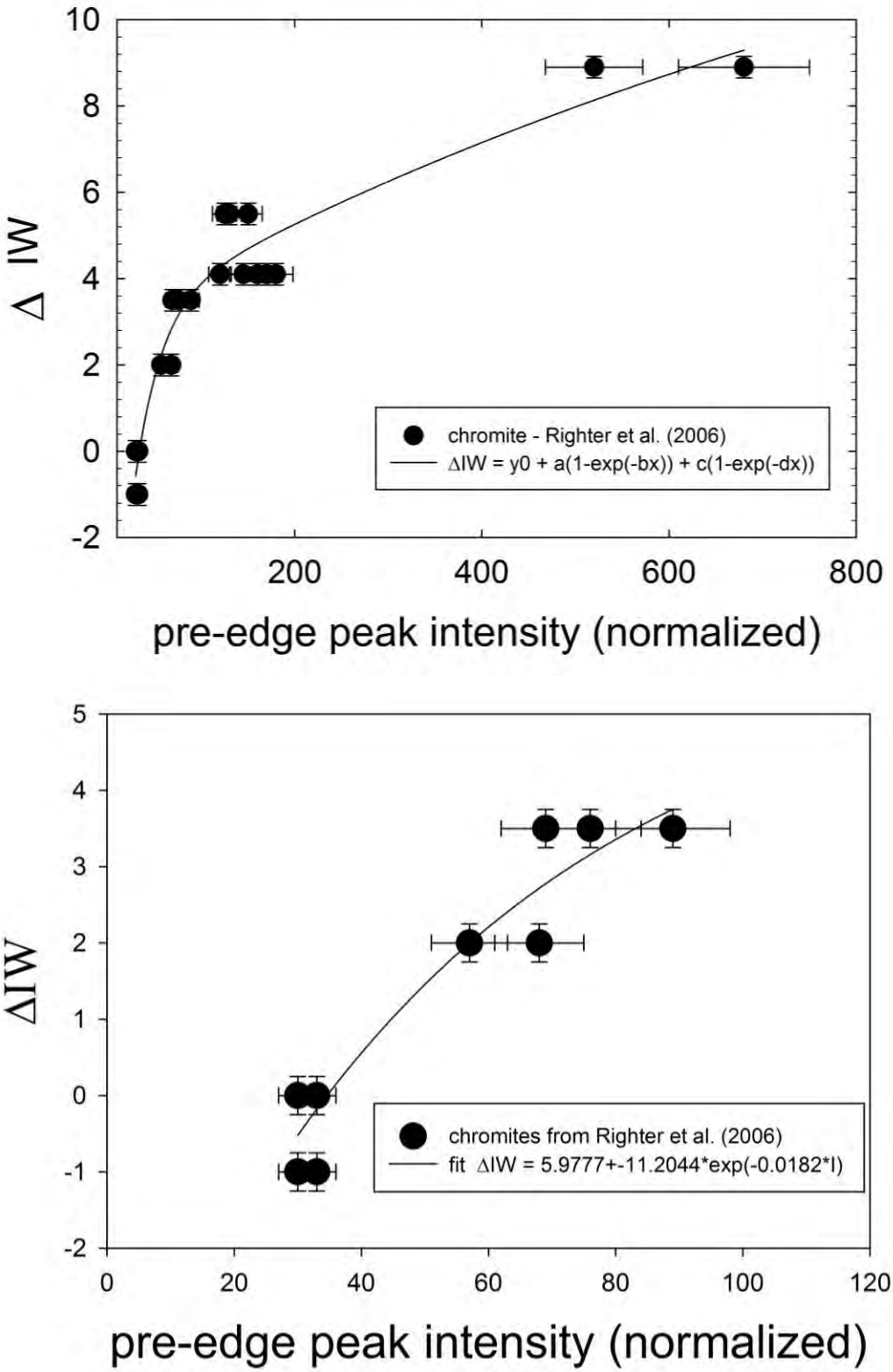

Figure 2

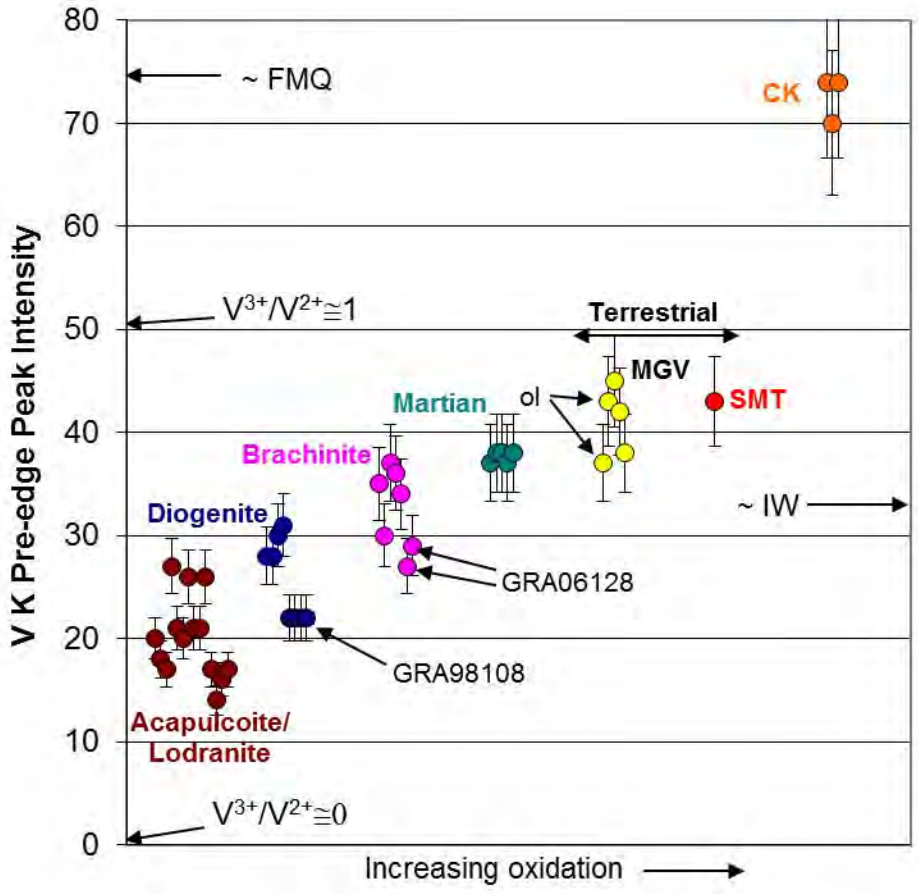

Figure 3

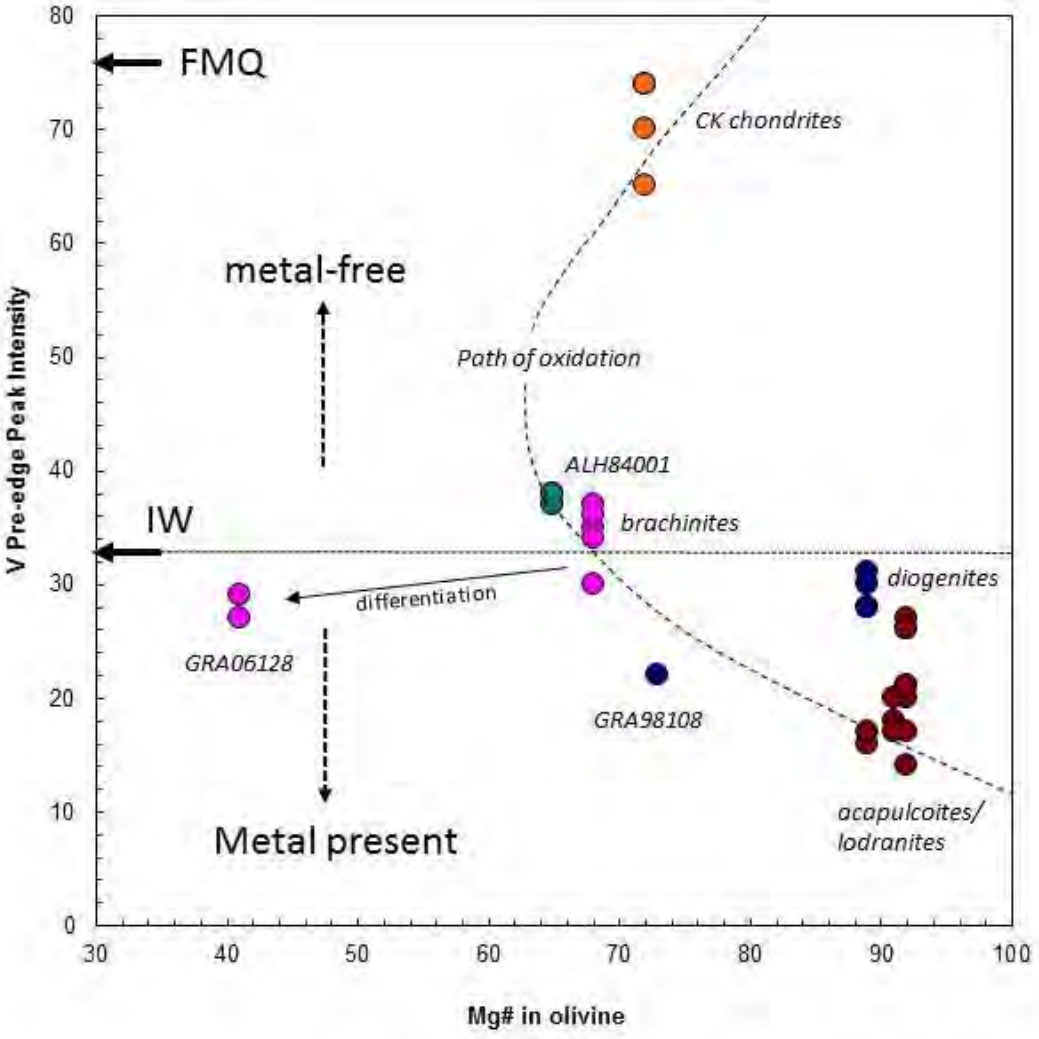

Figure 4

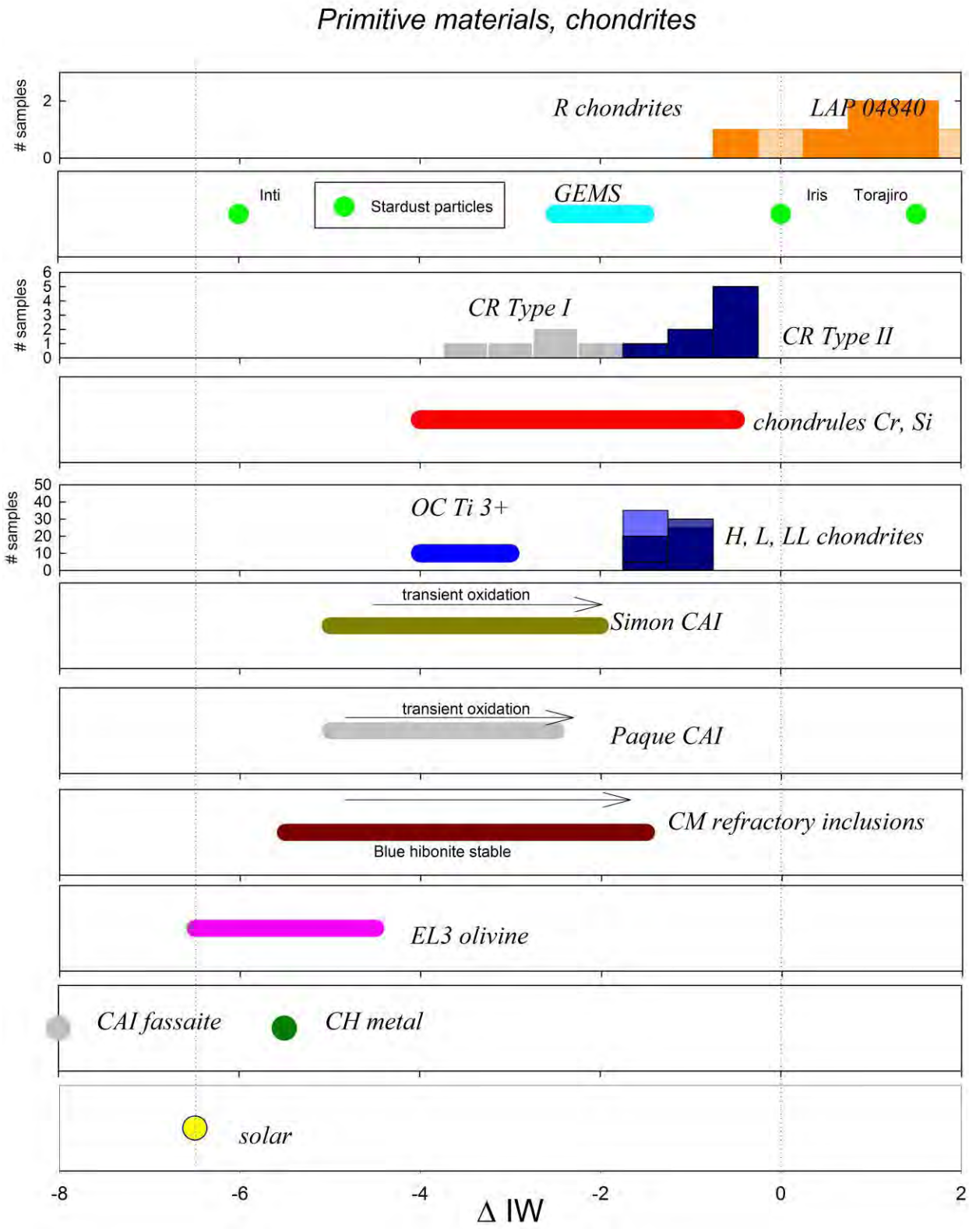

Figure 5

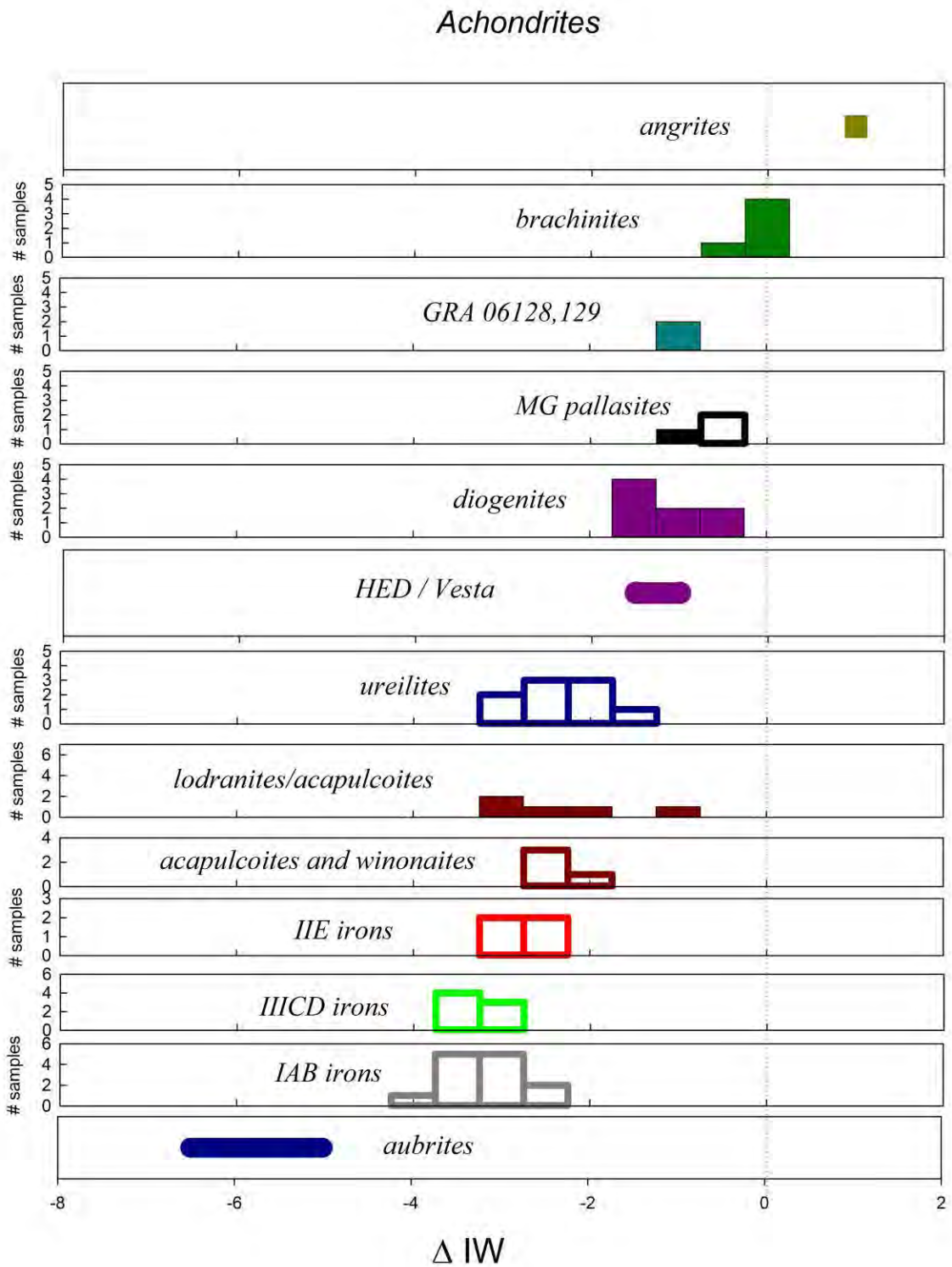

Figure 6

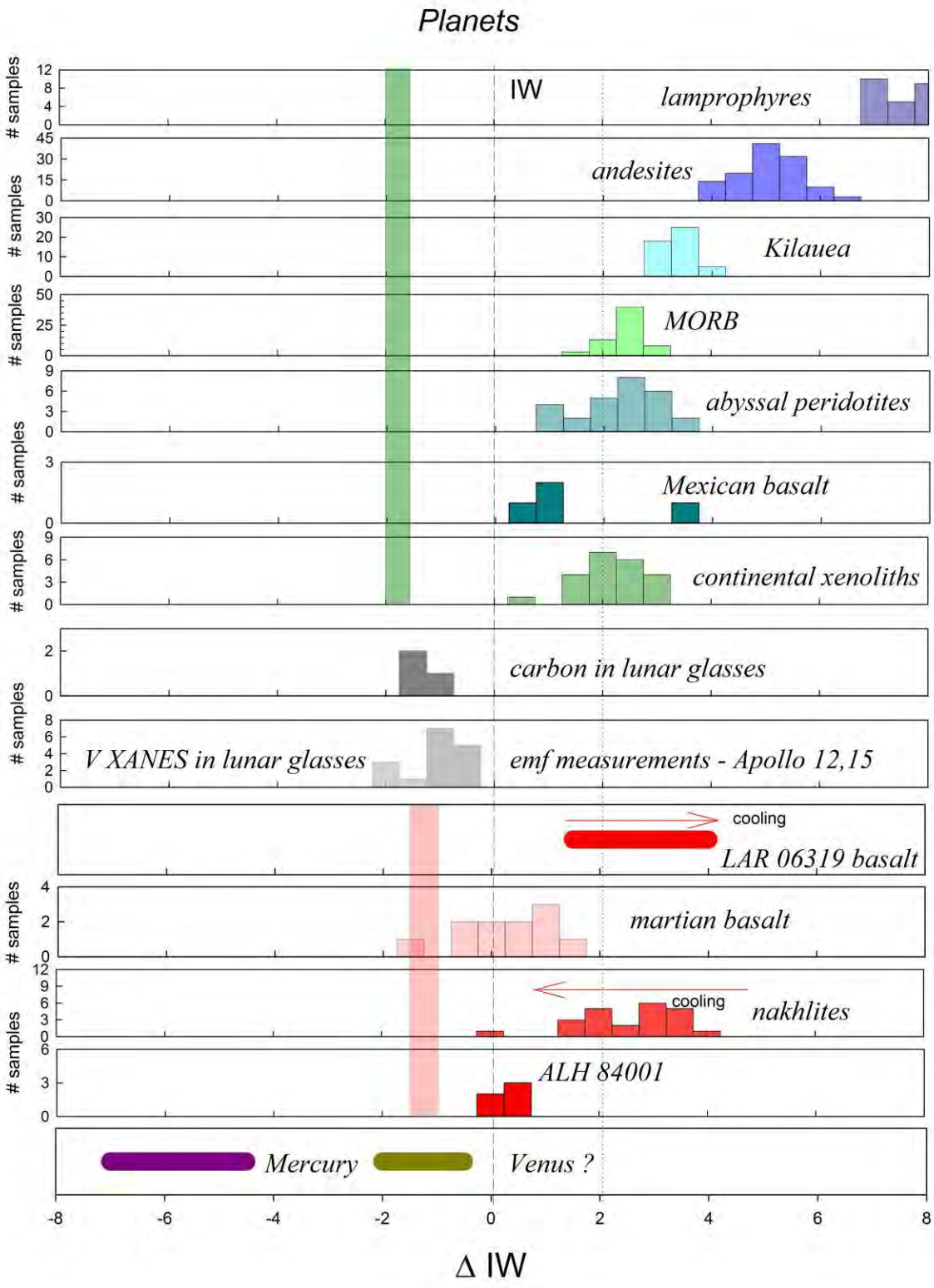

Figure 7

Table 1: Results of V XANES measurements for individual spinel-structured oxides

sample	*Section #*	*type*	*Pre-edge peak intensity*	*ΔIW* [1]	*ΔIW* [2]
ALH77256_1.002-4	116	olivine diogenite	28(3)	-0.88	-0.75
ALH77256_2.001-3	116	olivine diogenite	28(3)	-0.88	-0.75
ALH77256_3.001-3	116	olivine diogenite	30(3)	-0.56	-0.51
ALH77256_4.001-3	116	olivine diogenite	31(3)	-0.41	-0.41
GRA98108_md2.001-3	17	olivine diogenite	22(2)	-1.98	-1.53
GRA 98108_md1.001-3	17	olivine diogenite	22(2)	-1.98	-1.53
GRA98108_brd1.001-3	17	olivine diogenite	22(2)	-1.98	-1.53
GRA 98108_ah1.001-3	17	olivine diogenite	22(2)	-1.98	-1.53
ALH84025_1.004-5	12	brachinite	35(4)	0.15	0.05
ALH84025_2.001-3	12	brachinite	30(3)	-0.56	-0.51
EET99402_1.003-4	33	brachinite	37(4)	0.41	0.26
EET99402_2.001-3	33	brachinite	36(4)	0.28	0.16
EET99402_3.001-3	33	brachinite	34(3)	0.02	-0.06
CMS04071_2.001	9	pallasite	27(3)	-1.05	-0.88
QUE99679_1.002-4	7	CK4 chondrite	74(7)	3.11	3.06
QUE99679_2.001,2,4	7	CK4 chondrite	65(7)	2.70	2.55
QUE99679_3.001,2,3	7	CK4 chondrite	70(7)	2.94	2.84
QUE99679_4.001,2,3	7	CK4 chondrite	74(7)	3.11	3.06
SMT-1_grain1.004-6	-	Basalt	52(5)	1.07	0.85
MGV-19_ol_1.001-3	-	Basalt	37(4)	0.41	0.26
MGV-19_ol_3.001-3	-	Basalt	43(4)	1.08	0.85
TMV-6b_ol_3.001-3	-	Basalt	82(8)	3.42	3.46
ALH84001_op1.001-2	382	Martian opx	37(4)	0.41	0.26
ALH84001_ht1.001-2	382	Martian opx	38(4)	0.53	0.37
ALH84001_ht2.001-2	382	Martian opx	38(4)	0.53	0.37
ALH84001_cy1.001-3	382	Martian opx	37(4)	0.41	0.26
ALH84001_cy2.001-3	382	Martian opx	38(4)	0.53	0.37
GRA 06128_wnr2.001-3	52	Ungr. achondrite	27(3)	-1.05	-0.88
GRA 06128_wnr2.001-3	52	Ungr. achondrite	29(3)	-0.72	-0.63
MET01198_wdg.001	14	acapulcoite	20(2)	-2.40	-1.81
MET01198_nja2.001	14	acapulcoite	18(2)	-2.85	-2.11
MET01198_nja1.001	14	acapulcoite	17(2)	-3.09	-2.25
EET84302_vst.002-3	44	lodranite	27(3)	-1.05	-0.88
EET84302_crg.002	44	lodranite	21(2)	-2.19	-1.68

LAP04840_wty1.003-6	24	R6 chondrite	30(3)	-0.56	-0.51
LAP04840_tub1.002-4	24	R6 chondrite	39(4)	0.64	0.47
LAP04840_snd1.001-3	24	R6 chondrite	49(5)	1.63	1.38
LAP04840_lzy1.001-3	24	R6 chondrite	37(4)	0.40	0.26
LAP04840_ftd1.001-3	24	R6 chondrite	41(4)	0.87	0.66
LAP04840_flndr1.001-3	24	R6 chondrite	46(5)	1.36	1.13

1 - fit to a five parameter exponential function across IW-1 to IW+9; std error = 0.78.
2 - fit to exponential function between IW-1 and IW+4; std error = 0.62.

- ΔIW refers to the $\log fO_2$ of a sample (at T) relative to the $\log fO_2$ of the IW buffer (at T).